SE

ORT DOCUMENTATION PAGE

1a AD-A204 219

1b. RESTRICTIVE MARKINGS

2a

3. DISTRIBUTION / AVAILABILITY OF REPORT
Approved for public release;
Distribution unlimited

2b. DECLASSIFICATION / DOWNGRADING SCHEDULE

4. PERFORMING ORGANIZATION REPORT NUMBER(S)

5. MONITORING ORGANIZATION REPORT NUMBER(S)
EOARD

6a. NAME OF PERFORMING ORGANIZATION
Ben Gurion University of the Negev

6b. OFFICE SYMBOL (If applicable)

7a. NAME OF MONITORING ORGANIZATION
European Office of Aerospace Research and Development

6c. ADDRESS (City, State, and ZIP Code)
Department of Mechanical Engineering
P.O.B. 653
Beer Sheva 84 105, Israel

7b. ADDRESS (City, State, and ZIP Code)
Box 14
FPO New York 09510-0200

8a. NAME OF FUNDING / SPONSORING ORGANIZATION European Office of Aerospace Research & Development

8b. OFFICE SYMBOL (If applicable)
LRC

9. PROCUREMENT INSTRUMENT IDENTIFICATION NUMBER
AFOSR 86-0349

8c. ADDRESS (City, State, and ZIP Code)
Box 14
FPO New York 09510-0200

10. SOURCE OF FUNDING NUMBERS

PROGRAM ELEMENT NO.	PROJECT NO.	TASK NO.	WORK UNIT ACCESSION NO.
61102F	2301	D1	

11. TITLE (Include Security Classification) A NUMERICAL INVESTIGATION OF THE FLOW FIELD DEVELOPED BEHIND (A) AN OBLIQUE SHOCK WAVE PROPAGATING INTO A DUSTY GAS, (B) A NORMAL SHOCK WAVE PROPAGATING INTO A DUSTY GAS HAVING DUST PARTICLES OF VARIOUS SIZE

12. PERSONAL AUTHOR(S) Professors G. Ben-Dor and O. Igra

13a. TYPE OF REPORT	13b. TIME COVERED	14. DATE OF REPORT (Year, Month, Day)	15. PAGE COUNT
Final Scientific	FROM 1 Sep86 TO 31Aug88	1988 October	

16. SUPPLEMENTARY NOTATION

17. COSATI CODES			18. SUBJECT TERMS (Continue on reverse if necessary and identify by block number)
FIELD	GROUP	SUB-GROUP	Dusty Shock Waves, Solid-Gas Suspensions, Two Phase Flows

19. ABSTRACT (Continue on reverse if necessary and identify by block number)

The dependence of the shock induced flow field on non-uniformities of the various physical properties of the dust (namely, the diameter, the material density and the heat capacity) were investigated numerically. The flow field which is developed when a dusty gas steady suspension passes through an oblique shock wave was investigated numerically. In addition, the dependence of the shock induced flow field on the various physical properties of the dust was investigated.

20. DISTRIBUTION / AVAILABILITY OF ABSTRACT
☒ UNCLASSIFIED/UNLIMITED ☐ SAME AS RPT. ☐ DTIC USERS

21. ABSTRACT SECURITY CLASSIFICATION
Unclassified

22a. NAME OF RESPONSIBLE INDIVIDUAL	22b. TELEPHONE (Include Area Code)	22c. OFFICE SYMBOL
CHESTER J. DYMEK, JR, Lt Col, USAF	(44 1) 409-4384	EOARD/LRC

DD FORM 1473, 84 MAR 83 APR edition may be used until exhausted. All other editions are obsolete.

SECURITY CLASSIFICATION OF THIS PAGE

EOARD-TR-89 06

This report has been reviewed by the EOARD Information Office and is releasable to the National Technical Information Service (NTIS). At NTIS it will be releasable to the general public, including foreign nations.

This technical report has been reviewed and is approved for publication.

CHESTER J. DYMEK, JR., Lt Col, USAF
Chief, Chemistry

FRED T. GILLIAM, Lt Col, USAF
Chief Scientist

Accession For	
NTIS GRA&I	☒
DTIC TAB	☐
Unannounced	☐
Justification	
By	
Distribution/	
Availability Codes	
Dist	Avail and/or Special
A-1	

A Numerical Investigation of the Flow Field Developed Behind a) An Oblique Shock Wave Propagating into a Dusty Gas b) A Normal Shock Wave Propagating into a Dusty Gas Having Dust Particles of Various Size

Final Report

Prof. G. Ben-Dor

Prof. O. Igra

Period: Oct. 1, 1986 - Sept. 30, 1988

Contract: AFOSR-86-0349

Introuction

Since the research project consists of two parts, this final report is also divided into the corresponding two parts. The first part summarizes our numerical results on the flow of a dust-gas suspension through an oblique shock wave, and the second part deals with the flow of a dust-gas suspension having various distributions of the properties of the dust particles through a normal shock wave.

Part I

The Flow of a Dust-Gas Suspension Through an Oblique Shock Wave

Abstract

The equations governing the flow field which is developed when a supersonic dusty-gas suspension passes through a straight oblique shock wave were formulated. A computer code for solving the governing equations was developed and used to obtain the solution for a variety of different initial conditions.

In addition, the dependence of the post-shock suspension properties on the various physical properties of the dust particles, (namely the diameter of the dust particles, their specific heat capacity, their material density and the loading ratio of the dust in the suspension) was investigated.

Nomenclature

- A - envelope area of the solid particle = πD^2
- C - specific heat capacity of the solid particle
- C_D - drag coefficient
- C_p - specific heat capacity at constant pressure of the gaseous phase
- C_v - specific heat capacity at constant volume of the gaseous phase
- D - diameter of the solid particle
- F_D - drag force
- k - thermal conductivity
- M - flow Mach number
- m_p - mass of a solid particle
- Nu - Nusselt number
- n - a co-ordinate normal to the oblique shock wave
- n_p - number density of the solid particles
- P - suspension pressure
- Pr - Prandtl number

$Q_{H.T.}$ - rate of heat per unit volume transferred from the gaseous to the solid phase
R - specific gas constant
Re - Reynolds number
S - cross section of the solid particle = $\pi D^2/4$
T - temperature
u - velocity of gaseous phase
v - velocity of the solid phase

γ - specific heat capacities ratio = C_p/C_v
ϕ - angle of incidence
θ - flow deflection angle
μ - dynamic viscosity
ρ - spatial density
σ - material density
η - loading ratio of the solid phase in the suspension = ρ_{p_0}/ρ_{g_0}

Subscripts

g - gaseous phase
n - normal component
p - solid phase
s - tangential component
x - horizontal co-ordinate
y - vertical co-ordinate
0 - flow state ahead of the shock wave
1 - flow state behind the shock wave

Introduction

The interest in the gas-dynamic behaviour of a gas-particle suspension grew in the past three decades due to its application to many engineering problems. Some typical examples are: metallized propellents of rockets, jet-type dust collectors and blast waves in dusty atmospheres. In addition, mixtures with gases heavily laden with particles occur frequently in industrial processes such as plastics manufacturing, flour milling, coal-dust conveying, powder metallurgy and powdered-food processing. General

descriptions of such flows can be found in several books and review papers [Soo (1967), Marble (1970) and Rudinger (1973)]

The major differences between the flow fields which are developed behind a normal shock wave in a dusty-gas and a pure (dust-free) gas are illustrated in figures 1a and b for the temperatures and the velocities, respectively. When a steady pure gas encounters a normal shock wave it experiences a sharp (almost discontinuous) change in its thermodynamic and kinematic properties. This sudden change is shown in figure 1 to occur between (0) and (1). The thickness of this disturbance, l_f, is only a few mean free paths of the gas atoms or molecules (about 6.6×10^{-6} cm in standard conditions). Beyond (1) the gas properties remain constant (solid lines in figures 1a and b) provided the gas conditions at (1) are not sufficient to excite the internal degrees of freedom of the gas.

If, however, the gas is laden with solid particles then the suspension which was originally at a state of thermodynamic and kinematic equilibrium, ahead of the shock front, is suddenly changed into a non-equilibrium state, because the solid particles, due to their size compared with l_f, do not experience any noticeable change in their properties upon moving from (0) to (1). Thus, at (1) the gas has a much higher temperature than the dust, $T_g >> T_p$ and a much lower velocity $u << v$. Morgenthaler (1962) indicated that this is true even if the particle diameter is as small as 0.1 μm (for shock waves in air at nearly standard conditions, where the mean free path is about 0.066 μm). Therefore, the particles are not influenced by the initial disturbance, and the gas properties at (1) can be safely assumed to be identical to those of a pure gas with the same initial conditions.

Far downstream of (1), i.e., at (∞) in figure 1, the gas and the solid phases reach a new state of thermodynamic and kinematic equilibrium via momentum and energy exchange. Theoretically all shock waves in dusty gases are infinitely thick, since equilibrium is approached asymptotically. However, it is a common practice to assign to the shock wave an effective thickness which is defined by a requirement that the suspension properties come close to their equilibrium downstream values. It was shown by Gottlieb & Coskunses (1985) that the suspension equilibrium properties (at infinity) can be calculated from the usual normal shock wave relations,

provided that the usual pure gas parameters $\bar{\gamma}$ and $\bar{R}$ (the specific heat capacities ratio and the specific gas constant) are replaced by effective values γ and R which solely depend on the initial conditions of the suspension.

Between (1) and (∞) the solid particles are not in equilibrium with the gas. The flow region between (1) and (∞) is known as the relaxation zone, for it is analogous to the relaxation zone in pure gases where the internal degrees of freedom are excited. The extent of the relaxation zone strongly depends on the momentum and heat transfer mechanisms which enable the solid and the gaseous phases to reach a new equilibrium state. The analysis of the relaxation zone was studied by many investigators. The pioneering works of Carrier (1958), Kriebel (1964) and Rudinger (1964) verified the existence of this relaxation zone and identified the parameters affecting it, namely; the solid particle diameter, D, its specific heat capacity, C, its material density, σ, and the loading ratio, η. Igra & Ben-Dor (1980) compared various correlations for the drag coefficient, C_D, and the heat transfer coefficient, Nu, and pointed out their effect on the extent of the relaxation zone. In addition they studied the role of thermal radiation heat transfer between the two phases and showed that it can be neglected when the incident shock waves Mach number is smaller than five.

In all the above mentioned works, as well as in many others, the gaseous phase was assumed to behave as a perfect gas. This assumption was relaxed by Ben-Dor & Igra (1982) and Igra & Ben-Dor (1984) who solved the flow field while accounting for real gas effects. Dissociating nitrogen was the gaseous phase in the latter work and ionizing argon in the former.

The assumption that the solid particles are inert, which was also adopted in most of the published studies, was relaxed by Elperin, Ben-Dor & Igra (1986) who solved the flow field of an oxygen-carbon suspension passing through a normal shock wave, behind which the temperature of the carbon particles reached their ignition temperature and burned out.

The assumption of uniform solid particles was relaxed by Elata, Ben-Dor & Igra (1988) who solved the case of size-distributed solid particles.

In all the above mentioned solutions the flow field was one-dimensional and steady. The aim of the present study was to solve the case of a two-dimensional steady flow. This is the case when the shock wave is

oblique. There are many incidences where the shock wave is oblique. For example, one can mention the shock wave generated by a supersonic vehicle, the shock wave which is developed at the entrance nozzle of a rocket engine and the reflected shock waves which arise when an explosion generated blast wave interacts with man-made structures. In all these cases the shock wave is oblique and, hence, unlike the previously mentioned cases the resulted flow field behind the shock wave is two-dimensional.

The aim of the present study, therefore, is to solve the flow field which is developed when a supersonic dusty gas suspension passes through a straight oblique shock wave.

Figure 2 illustrates schematically the problem to be solved. A dust gas suspension which is in a thermal and kinematic equilibrium encounters an oblique shock wave. The angle of incidence is ϕ (sometimes known as the wave angle). As mentioned previously, upon the passage of the suspension through the shock wave, the properties of the gaseous phase assume a new state, known as the frozen state, immediately behind the shock front, while the solid phase passes through the shock wave unaffected. Due to the fact that the shock wave is oblique, the streamline of the gaseous phase is deflected by an angle, θ_g, while the trajectory of dust particles remains unchanged. Thus, in addition to the differences in the properties of the two phases which were mentioned previously, here there is also a difference in the direction of propagation of the two phases. The two phases which are no longer in equilibrium, start exchanging momentum and energy until they finally reach a new thermal and kinematic equilibrium. Here, kinematic equilibrium means that, in addition to equal velocities, the two phases also reach the same direction. The flow region inside which the two phases are in non-equilibrium, i.e., the relaxation zone, is also shown in figure 2.

Theoretical Background

Assumptions

The assumptions upon which the present model is based and their implications are listed in the following:

1) The gaseous phase behaves as an ideal gas. Thus, the equation of state of the gas is $P = \rho_g R T_g$. Note that it is not assumed here that the gas is

calorically ideal. Alternatively, the dependence of both C_p and C_v on the gas temperature is accounted for. This has not been done in previous studies where both C_p and C_v were assumed to be constant.

2) All solid particles are rigid, inert small identical spheres uniformly distributed in the gaseous phase. Thus there is no heat addition or reduction due to chemical processes between the solid and the gaseous phases. Furthermore, Re and Nu are based on the particle diameter, D.
3) The volume of the solid phase in the suspension can be neglected. Thus the momentum and energy exchange among the solid particles can be ignored.
4) Aside from momentum and energy interactions between the gaseous and the solid phases, the gaseous phase is considered to be a perfect flow, i.e., the dynamic viscosity, μ_g, and the thermal conductivity, k_g, are zero. This also implies that neither kinematic nor thermal boundary layers develop around the solid particles.
5) The dynamic viscosity, μ_g, the thermal conductivity, k_g, and the specific heat capacity at constant pressure, C_p, of the gaseous phase depend solely on its temperature, T_g.
6) The solid particles are too large to experience any change in their thermodynamic and dynamic properties upon their passage through the shock front. In addition they are also large enough not to experience Brownian motion. Thus, the partial pressure of the solid phases can be neglected.
7) The solid particles are small enough to satisfy the condition $B_i < 0.1$, where B_i is the Biot number, $B_i = hr/k_p$ (h is the coefficient of connection heat transfer, r is the radius of the solid particle, and k_p is its thermal conductivity). Thus the temperature within the solid particles can be assumed to be uniform.
8) The weight of the solid particles and the buoyancy forces experienced by them are negligibly small in comparison with the drag forces acting on them.
9) The specific heat capacity, C, of the solid particles is constant.
10) Ahead of the normal shock wave the suspension is at a state of thermodynamic and kinematic equilibrium, i.e., $u_0 = v_0$ and $T_{g0} = T_{p0}$, where u and v are the velocities of the gas and the solid particles, and

T_g and T_p are the temperatures of the gaseous and solid phases, respectively.

11) Based on the density ratio of the two phases 1/2500, the virtual mass which depends on this ratio is neglected.

In addition to the above listed assumptions it is assumed that the flow field under consideration is two-dimensional and steady.

If the entire problem is analyzed in the (s,n)-plane, where the s-axis is parallel to the shock wave front and the n-axis is normal to the shock wave front, then the problem at hand can be considered as one-dimensional. Note that the s-component of the velocities of the two phases immediately behind the shock front are identical, i.e., $u_{1s} = v_{1s}$. For this reason the relative velocity between the two phases in the s-direction is zero, and therefore there are no drag forces in the s-direction. As a consequence, there are no changes in the velocity components in the s-direction and they remain constant in the entire flow field. From symmetrical considerations, it is obvious that all the properties of the suspension must remain constant along n=constant lines, i.e., along lines which are parallel to the s-axis. Therefore, the partial derivative of any of the suspension properties with respect to s is zero.

Governing Equations

Based on the foregoing discussion and assumptions, the governing equations for the problem at hand are:

- conservation of mass of the gaseous phase:

$$\frac{d}{dn}(\rho_g u_n) = 0 \qquad (1)$$

- conservation of mass of the solid phase:

$$\frac{d}{dn}(\rho_p v_n) = 0 \qquad (2)$$

- conservation of linear momentum of the gaseous phase:

$$\rho_g u_n \frac{du_n}{dn} + \frac{dP}{dn} = F_{Dn} \tag{3}$$

- conservation of linear momentum of the solid phase:

$$\rho_p v_n \frac{dv_n}{dn} = -F_{Dn} \tag{4}$$

- conservation of energy of the gaseous phase:

$$\rho_g u_n \frac{d}{dn}(C_p T_g + \frac{1}{2} u_n^2) = Q_{H.T.} + F_{Dn} v_n \tag{5}$$

- conservation of energy of the solid phase:

$$\rho_p v_n \frac{d}{dn}(C T_p + \frac{1}{2} v_n^2) = -Q_{H.T.} - F_{Dn} v_n \tag{6}$$

where ρ_g and ρ_p are the spatial densities of the gaseous and solid phases, u_n and v_n are the velocity components of the gaseous and solid phases in the n-direction, T_g and T_p are the temperatures of the gaseous and solid phases, P is the pressure of the suspension, C_p is the specific heat capacity at constant pressure of the gaseous phase, C is the specific heat capacity of the solid particles, $Q_{H.T}$ is the amount of heat transferred per unit volume from the gaseous phase to the solid phase and F_{Dn} is the drag force per unit volume applied by the gaseous phase on the solid particles.

Thus, if C_p, C, $Q_{H.T}$ and F_{Dn} are expressed in terms of the dependent variables namely; ρ_g, ρ_p, u_n, v_n, T_g, T_p and P, then the above set of six conservation equations contain seven unknowns. The seventh equation which is required to make the above set of equations solvable, is the equation of state of the gaseous phase; i.e.,

$$P = \rho_g R T_g \tag{7}$$

In the following, the above mentioned complementary equations are developed.

The drag force per unit volume can be obtained by multiplying the drag force acting on a single solid particle by the number density of the solid particles.

$$F_{Dn} = \frac{1}{2} \rho_g C_D (v_n - u_n) \cdot |v_n - u_n| \cdot S \, n_p \qquad (8)$$

where C_D is the drag coefficient, S is the projected cross section of the solid spherical particle (i.e., $S = \pi D^2/4$, where D is the diameter of the solid particles), and n_p the number density of the solid particles can be calculated from

$$n_p = \frac{\rho_p}{m_p} \qquad (9)$$

where m_p is the mass of a single solid particle (i.e., $m_p = \sigma \pi D^3/6$, where σ is the material density of the solid particles).

The drag coefficient, C_D, is usually expressed as a function of the Reynolds number, Re, which in turn depends on the slip velocity $|v_n - u_n|$. For this reason, the Re number is very high immediately behind the shock wave while its magnitude vanishes towards the end of the relaxation zone, where $v_n \approx u_n$, is approached. For this reason two different correlations for the drag coefficient C_D are used:
For $Re < 800$

$$C_D = \frac{24}{Re} (1 + 0.15 \, Re^{0.687}) \qquad (10a)$$

and for $800 < Re < 3 \times 10^5$

$$C_D = \frac{24}{Re} (1 + 0.15 \, Re^{0.687}) + \frac{0.42}{1 + 42500 \; Re^{-1.16}} \qquad (10b)$$

Both of these correlations were taken from Clift, Grace & Weber (1978). The Reynolds number is calculated from:

$$Re = \frac{\rho_g |v_n - u_n| D}{\mu_g} \qquad (11)$$

where μ_g, the dynamic viscosity of the gaseous phase, is calculated by the expression suggested by Mazor, Ben-Dor & Igra (1985) which reads:

$$\mu_g = \mu_{g_r} \left(\frac{T_g}{T_{g_r}} \right)^{0.65} \qquad (12)$$

where μ_{g_r} is the dynamic viscosity of the gaseous phase at a reference temperature T_{g_r}.

The heat transferred per unit volume from the gaseous phase to the solid phase can be obtained by multiplying the heat transferred to a single particle by the number density of the solid particles, i.e.,

$$Q_{H.T} = Ah(T_p - T_g)n_p \qquad (13)$$

where A is the surface area of the solid spherical particle (i.e., $A = \pi D^2$) and h the coefficient of heat convection can be calculated from

$$h = \frac{Nuk_g}{D} \qquad (14)$$

where k_g is the thermal conductivity of the gaseous phase and Nu the Nusselt number is a function of the Reynolds number, Re, and the Prandtl number, Pr, which is defined as

$$Pr = \frac{\mu_g \, C_p}{k_g} \qquad (15)$$

The correlation for Nu which was used in the present study is taken from Drake (1961). It reads:

$$Nu = 2 + 0.459 \, Pr^{1/3} \, Re^{0.55}$$

As mentioned in assumption (5) the specific heat capacity at constant pressure, C_p, and the thermal conductivity, k_g, depend solely on the temperature of the gaseous phase, T_g. For this reason the gaseous phase was identified as air. For air (Holman, 1981, p. 542) in the range
$300 < T_g < 2500K$

$$k_g = 0.0125 + 5.509 \times 10^{-5} T_g \qquad (16)$$

and from Van Wylen & Sonntag (1978) p. 683

$$C_p = 39.06 - 512.79 \left(\frac{T_g}{100}\right)^{-1.5} + 1072.7 \left(\frac{T_g}{100}\right)^{-2} - 820.4 \left(\frac{T_g}{100}\right)^{-3}$$

this condition is good for $300 < T_g < 3500$ K.

Numerical Solution

Now we are at the stage where the governing equations are well defined, i.e., the number of independent variables is equal to the number of equations and all the non-dependent variables can be expressed in terms of the dependent variables and other known parameters.

As can be seen, the governing equations of the problem at hand consist of seven non-linear differential equations which must be solved simultaneously in order to obtain the spatial distribution of the flow properties.

Numerous computer code packages, capable of numerically solving non-linear differential equations, are available, e.g., the IMSL (International Mathematical and Statistical Libraries). This package contains three different computer codes for solving a given set of differential equations provided the initial conditions are known. (As will be shown subsequently, the initial conditions in the case at hand are indeed known.) The most accurate code out of these three codes is DREBS. It is based on the extrapolation method, and is superior when very high accuracy is required and when the calculation of the derivatives is not expensive.

Fortunately, the relative simplicity of the governing equations of the problem at hand, enables one to rewrite them in a form where the

derivatives of the dependent variables are isolated, and hence can be calculated very quickly and cheaply (computer-wise). The rewritten set of the governing equations can be changed to the following form:

$$\frac{dT_g}{dn} = \frac{Q_{H.T.} + F_D v - \frac{F_D u^3}{u^2 - RT_g}}{\rho_g u \left[C_p - \frac{R u^2}{u^2 - RT_g} \right]} \tag{17}$$

$$\frac{du}{dn} = \frac{F_D - \rho_g R \frac{dT_g}{dn}}{\rho_g \frac{u - RT_g}{u}} \tag{18}$$

$$\frac{dP}{dn} = \rho_g R \left(\frac{dT_g}{dn} - \frac{T_g}{u} \frac{du}{dn} \right) \tag{19}$$

$$\frac{d\rho_g}{dn} = - \frac{\rho_g}{u} \frac{du}{dn} \tag{20}$$

$$\frac{dT_p}{dn} = - \frac{Q_{H.T.}}{c \rho_p v} \tag{21}$$

$$\frac{dv}{dn} = - \frac{F_D}{\rho_p v} \tag{22}$$

$$\frac{d\rho_p}{dn} = - \frac{\rho_p}{v} \frac{dv}{dn} \tag{23}$$

The Initial Conditions

As mentioned earlier, the problem at hand is such that the initial conditions, i.e., the values of the dependent variables at $x = 0$ (at state (1) in figure 1) can be easily calculated.

Based on the fact that the thickness of the shock wave front is orders of magnitude smaller than the diameter of the solid particles, it is a common practice to assume that:

1. The gaseous phase experiences the well known "frozen" change upon its passage through the shock wave.

2. The solid phase remains unaffected as it passes through the shock wave.

The above assumptions imply that while the properties of the solid phase immediately behind the shock wave front are identical to those ahead of it, the properties of the gaseous phase can be calculated using the well known Rankine-Hugoniot relations which relate the gas properties in both sides of the shock wave. More specifically;

$$\rho_{g_1} = \rho_{g_0}\left[\frac{(\gamma+1)\,M_0^2}{(\gamma-1)\,M_0^2+2}\right] \tag{24}$$

$$P_1 = P_0\left[\frac{1}{\gamma+1}\,(2\,\gamma\,M_0^2 - \gamma + 1)\right] \tag{25}$$

$$T_{g_1} = T_{g_0}\left[\frac{\left(1+\frac{\gamma-1}{2}\,M_0^2\right)\left(\frac{2\gamma}{\gamma-1}\,M_0^2 - 1\right)}{\frac{(\gamma+1)^2}{2(\gamma-1)}\,M_0^2}\right] \tag{26}$$

$$M_1 = \frac{M_0^2 + \frac{2}{\gamma-1}}{\frac{2\gamma}{\gamma-1}\,M_0^2 - 1} \tag{27}$$

$$u_1 = M_1\sqrt{\gamma R T_{g_1}} \tag{28}$$

where subscripts "0" and "1" denote the flow states immediately ahead and behind the shock wave. M is the Mach number of the gaseous phase, i.e., $M = u/a$ (a, the local speed of sound, is simply calculated from $a = (\gamma R T)^{1/2}$).

Note that when $M_0 \to 1$, i.e., when the shock wave degenerates to a Mach wave, then there is no change in the properties of the gaseous phase as it passes through the shock wave.

Since the model at hand assumes that the gaseous phase behaves as a perfect gas the upper value of M_0 which can be used is limited, since as

$M_0 \to \infty$ $T_g \to \infty$. In the case of a diatomic gas, such as oxygen (O_2), nitrogen (N_2), etc., $M_0 = 6$ is usually taken as the upper limit for which the assumption of a perfect gas behaviour is valid. For monatomic gases such as helium (He), neon (Ne), argon (Ar), etc., the upper limit of M_0 is even higher. Beyond these limiting values, real gas effects must be accounted for. The ways of treating such cases are discussed by Ben-Dor and Igra (1982) and Igra and Ben-Dor (1984).

Complementary Equations

Once the set of the governing equations is solved, the velocity vectors of each of the two phases can be calculated from:

$$\vec{u} = u_n \hat{n} + u_s \hat{s} \tag{29a}$$

$$\vec{v} = v_n \hat{n} + v_s \hat{s} \tag{29b}$$

The absolute velocities of the two phase are therefore:

$$|\vec{u}| = (u_n^2 + u_s^2)^{1/2} \tag{30a}$$

$$|\vec{v}| = (v_n^2 + v_s^2)^{1/2} \tag{30b}$$

The deflection of the gaseous phase streamline, θ_g, from its original direction can be calculated from

$$\theta_g = \phi - \tan^{-1} \frac{u_n}{u_s} \tag{31a}$$

Similarly, the deflection of the dusty phase streamline, θ_p, is

$$\theta_p = \phi - \tan^{-1} \frac{v_n}{v_s} \tag{31b}$$

Obviously, when the suspension reaches a new equilibrium state at the end of the relaxation zone the flow directions of the two phases become parallel and hence $\theta_{g_{\infty}} = \theta_{p_{\infty}}$.

The velocity components of the gaseous and the dusty phases in the (x,y)-coordinate system shown in Figure 1 can be calculated from:

$$u_x = u_n \sin\phi + u_s \cos\phi \tag{32a}$$

$$u_y = -u_n \cos\phi + u_s \sin\phi \tag{32b}$$

and similarly for the solid phase:

$$v_x = v_n \sin\phi + v_s \cos\phi \tag{33a}$$

$$v_y = -v_n \cos\phi + v_s \sin\phi \tag{33b}$$

Numerical Results

As mentioned earlier, the problem at hand can be treated as one-dimensional by solving it in the (s,n)-plane. For this reason, the flow profiles shown in Igra and Ben-Dor (1980), for example, are all applicable for the case of oblique shock waves, provided the flow Mach number M_0 is replaced by $M_0 \sin\phi$ and the x-axis is replaced by the n-axis. Note that if the angle of incidence is set to $\phi = 90^0$, then the oblique shock wave becomes normal to the oncoming flow, and the general case of an oblique shock wave degenerates to the well known one-dimensional normal shock wave case.

Since the change of the flow properties in a direction normal to the oblique shock wave front as well as the dependence of these properties on the physical properties of the dust particles can be deduced from Igra and Ben-Dor (1980), in the following only results which are unique to the fact that the shock wave is oblique are presented.

The Gas Deflection - θ_g

As mentioned earlier, the direction of the streamline of the gaseous phase changes continuously from its "frozen" direction to its "equilibrium"

direction. In the following, the dependence of the flow deflection angle, θ_g, on the physical properties of the dust is discussed.

The dependence of the flow deflection, θ_g, on the dust loading ratio, η, is illustrated in figure 3, for $M_0 = 3$ and $\phi = 30^0$. The dust physical parameters are $D = 100\mu m$, $C = 1000J/(KgmK)$, $\sigma = 1500Kgm/m^3$.

As can be seen the frozen value of θ_g, i.e., θ_g at $n = 0$ is identical for all the cases. However, the larger the loading ratio is, the greater the equilibrium flow deflection becomes. The dashed lines are the values calculated by the equivalent gas concept presented in the introduction, which should be reached at the end of the relaxation zone.

It is also evident from figure 3 that the larger the loading ratio is, the shorter the relaxation length becomes. While for $\eta = 0.1$ it takes about 8m for the gaseous phase to reach the equilibrium deflection angle, only 3m are required when $\eta = 2$.

The deflection angle at the end of the relaxation zone, $\theta_{g_{eq}}$, as a function of the dust loading ratio, η, is shown in a different way in figure 4 for $M_0 = 4$, $\phi = 60^0$, $D = 100\mu m$, $C = 1000J/(KgmK)$ and $\sigma = 1500Kgm/m^3$.

The fact that the equilibrium deflection angle increases with increasing loading ratios is clearly seen in figure 4. However, it is evident that as η increases the rate of increase of the equilibrium deflection angle decreases and it seems that there is an upper limit on $\theta_{g_{eq}}$ as η assumes very high values.

The dependence of the deflection angle, θ_g, on the diameter of the solid particles is shown in figure 5. Again $M_0 = 3$ and $\phi = 30^0$. The dust properties are $\eta = 0.5$, $C = 1000J/(Kgm\ K)$ and $\sigma = 1500Kgm/m^3$.

Since the loading ratio, η, and the specific heat capacity of the dust particles, C, are the same for the cases, the equilibrium values at the end of the relaxation zone are identical. However, it is evident from figure 5 that the smaller the diameter of the solid particle is, the shorter the relaxation length becomes.

The dependence of the deflection angle, θ_g, on the specific heat capacity of the solid particles, C, for $M_0 = 3$ and $\phi = 30^0$ is shown in figure 6. The properties of the solid phase are $\eta = 0.5$, $D = 100\mu m$ and $\sigma = 1500Kgm/m^3$. It is evident from figure 6 that higher values of the specific heat capacities result in larger deflections at the end of the

relaxation zone. The length of the relaxation zone is not seen to strongly depend on the specific heat capacity.

The dependence of the deflection angle, θ_g, on the material density of the solid particles for $M_0 = 3$ and $\phi = 30^0$ is shown in figure 7. The dust properties are $\eta = 0.5$, $D = 100\mu m$, $C = 1000J/(Kgm\ K)$. Again, since η and C are identical for all the cases, the equilibrium values approached towards the end of the relaxation zone are the same for all the calculated cases. It is clearly seen from figure 7 that the smaller the material density is, the shorter the relaxation zone becomes. While it is about 4m for $\sigma = 1000Kgm/m^3$ it increases to about 10m when σ is increased to $2500Kgm/m^3$.

The gas and the solid particle paths is shown in figure 8 for $M_0 = 3$, $\phi = 60^0$, $\eta = 1.0$, $D = 100\mu m$, $C = 1000J/(Kgm\ K)$ and $\sigma = 1500Kgm/m^3$. The difference between the trajectories is clearly evident. While the gas particles are deflected immediately upon their passage through the shock wave (n=0), the solid particles do not change their original direction. However, behind the shock front the streamlines of the two phases approach a parallel direction. The results shown in figure 8 indicate that it is impossible to shape a wedge in a supersonic flow of a dusty gas, in such a way that it will generate a straight oblique shock wave. This is due to the fact that a straight oblique shock wave in a dusty gas results in two different particle trajectories, and no wedge can satisfy these two profiles. However, if the wedge surface is sticky, i.e., if it can be assumed that when a solid particle hits the surface, it sticks to it, then a wedge having a profile identical to that of the gas particle path might generate a straight oblique shock wave. It should be noted, however, that in the case of a sticky wedge surface, solid particles are drawn away from the suspension and hence their loading ratio η could be affected.

The dependence of the equilibrium deflection angle, $\theta_{g_{eq}}$, on the flow Mach number, M_0, is shown in figure 9 for $\phi = 60^0$, $\eta = 1$, $D = 200\mu m$, $C = 1000J/(Kgm\ K)$ and $\sigma = 1500Kgm/m^3$. It is evident from this figure that the equilibrium deflection angle increases as the flow Mach number increases. However, as the flow Mach number reaches high values, the equilibrium deflection angle is seen to approach an upper limit.

It is a common practice to use shock polars to study oblique shock waves. Thus, in the following, shock polars in dusty gas suspension are presented.

The (P,θ_g)-polar for the case $M_0 = 2.5$, $D = 100\mu m$, $C = 1000$ J/(Kgm K), $\sigma = 1500 Kgm/m^3$ and various values of η are shown in figure 10. The (P,θ_g)-polar in this case represents the conditions at the end of the relaxation zone, i.e., $P = P_{eq}$ and $\theta_g = \theta_{g_{eq}}$. As can be seen the equilibrium pressure, P_{eq}, becomes higher when η is increased. In addition, the maximum deflection angle, known as the detachment angle, is also seen to increase with increasing η. While for a dust-free (pure) gas (i.e., $\eta = 0$) $(\theta_{g_{eq}})_{max}$ is about 29^0, it reaches a value of about 56^0 when the loading ratio is $\eta = 2$.

A typical (ϕ, θ_g)-polar is shown in figure 11 for the same conditions of figure 10. Here again $\theta_g = \theta_{g_{eq}}$. It is evident from this figure that if a certain deflection is required, say 20^0, then as the loading ratio increases the angle of incidence, ϕ, which is needed to achieve the required deflection, decreases.

Conclusions

The flow field developed when a supersonic dusty gas suspension passes through a straight oblique shock wave has been investigated.

The investigation included a formulation of the governing equations of the flow field at hand and a numerical investigation of the dependence of the post shock suspension properties on the various physical properties of the solid particles.

Acknowledgement

The financial support received from the U.S. Air Force under Grant AFOSR-86-0349 is acknowledged with thanks.

List of References

Ben-Dor, G. and Igra, O., 1982, "The Relaxation Zone Behind Normal Shock Waves in a Dusty Reacting Gas, Part I: Monatomic Gases", Journal of Plasma Physics, Vol. 27, pp. 377-395.

Carrier, G.F., 1958, "Shock Waves in a Dusty Gas", Journal Fluid Mechanics, Vol. 4, pp. 376-382.

Clift, R., Grace, J.R. and Weber, M.E., 1978, "Bubbles, Drops and Particles", Academic Press, New York.

Drake, R.M., 1961, "Discussion on G.C. Vliet and G. Leppert Forced Convection Heat Transfer from an Isothermal Sphere to Water", ASME Journal Heat Transfer, Vol. 83, pp. 170-175.

Elata, D., Ben-Dor, G. and Igra, O., 1988, "The Effect of Particle Non-Uniformities of the Flow Field Behind Steady Normal Shock Waves", Submitted for publication.

Elperin, I., Ben-Dor, G. and Igra, O., 1986, "Analysis of Normal Shock Waves in a Carbon Laden Oxygen Gas", ASME Journal of Fluid Engineering, Vol. 108, pp. 354-359.

Gottlieb, J.J. and Coskunses, C.E., 1985, "Effects of Particle Volume on the Structure of a Partly Dispersed Normal Shock Wave in a Dusty Gas", UTIAS Report 295.

Igra, O. and Ben-Dor, G., 1980, "Parameters Affecting the Relaxation Zone Behind Normal Shock Waves in a Dusty Gas", Israel Journal of Technology, Vol. 18, pp. 159-168.

Igra, O. and Ben-Dor, G., 1984, "The Relaxation Zone Behind Normal Shock Waves in a Dusty Reacting Gas. Part 2: Diatomic Gases", Journal Plasma Physics, Vol. 31, pp. 115-140.

Kriebel, A.R., 1964, "Analysis of Normal Shock Waves in a Particle Laden Gas", Journal Basic Engineering, Transactions ASME, Ser. D86, pp. 655-665.

Marble, F.E., 1970, "Dynamics of Dusty Gases", Annual Review of Fluid Mechanics, Vol. 2, pp. 397-466.

Mazor, G., Ben-Dor, G. and Igra, O., 1985, "A Simple and Accurate Expression for the Viscosity of Diatomic Gases up to 10000K", AIAA Journal, Vol. 23, pp. 637-638.

Morgenthaler, J.H., 1962, "Analysis of Two-Phase Flow in Supersonic Exhausts", Progress in Astronautics and Aeronautics, Vol. 6, pp. 145-171.

Rudinger, G., 1973, "Wave Propagation in Suspension of Solid Particles in Gas Flow", Applied Mechanics Review, Vol. 26, pp. 273-279.

Rudinger, G., 1964, "Some Properties of Shock Relaxation in Gas Flow Carrying Small Particles", Physics of Fluids, Vol. 7, pp. 658-663.

Soo, S.L., 1967, "Fluid Dynamics of Multiphase Systems", 1967, Blaisdell Publishing Co., Waltham, Mass.

Van-Wylen, G.J. and Sonntag, R.E., 1978, "Fundamentals of Classical Thermodynamics", John Wiley & Sons, New York.

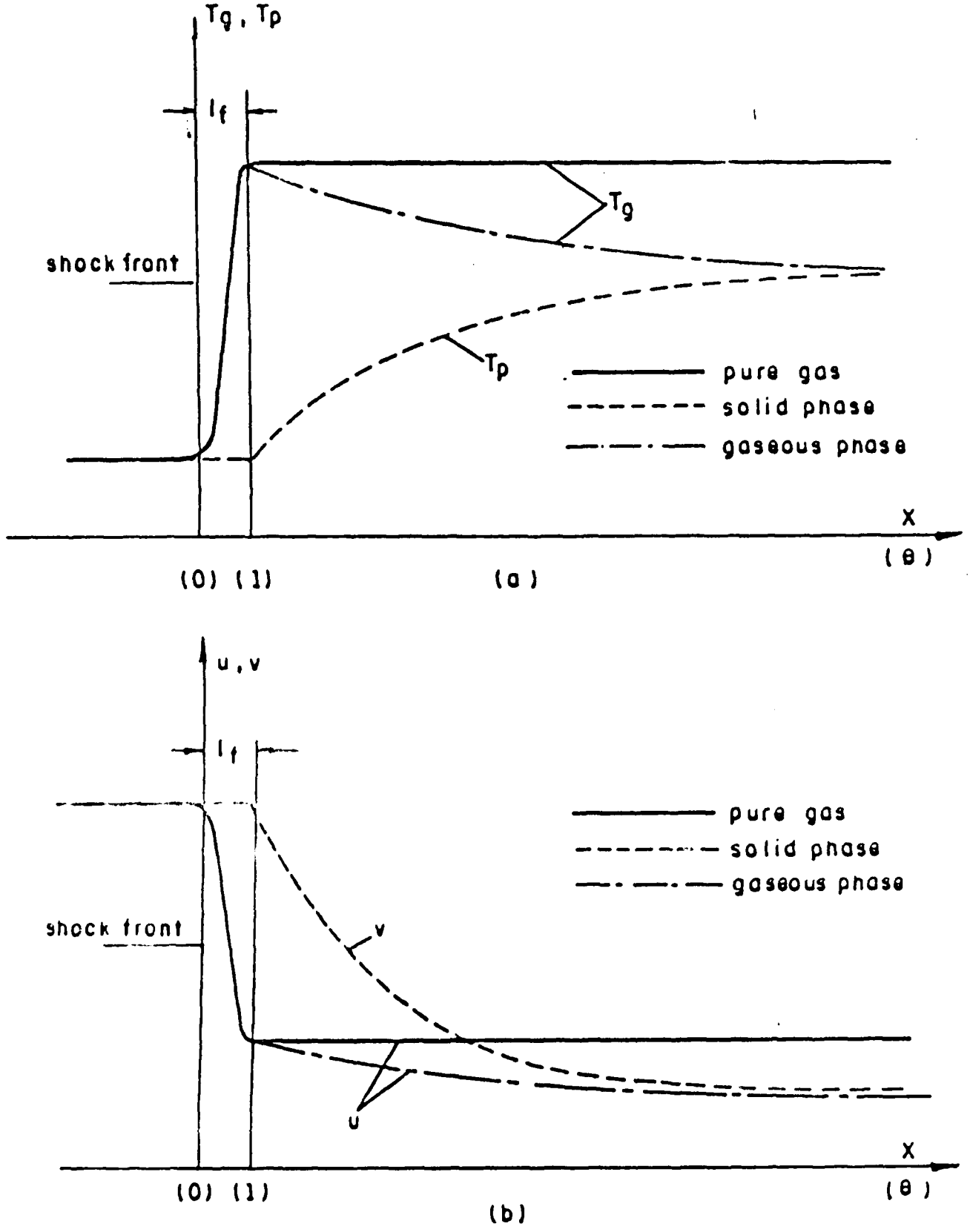

Figure 1: The shock wave structure in a pure (solid lines) and a dusty (dashed line) gas.
a) temperature profiles
b) velocity profiles

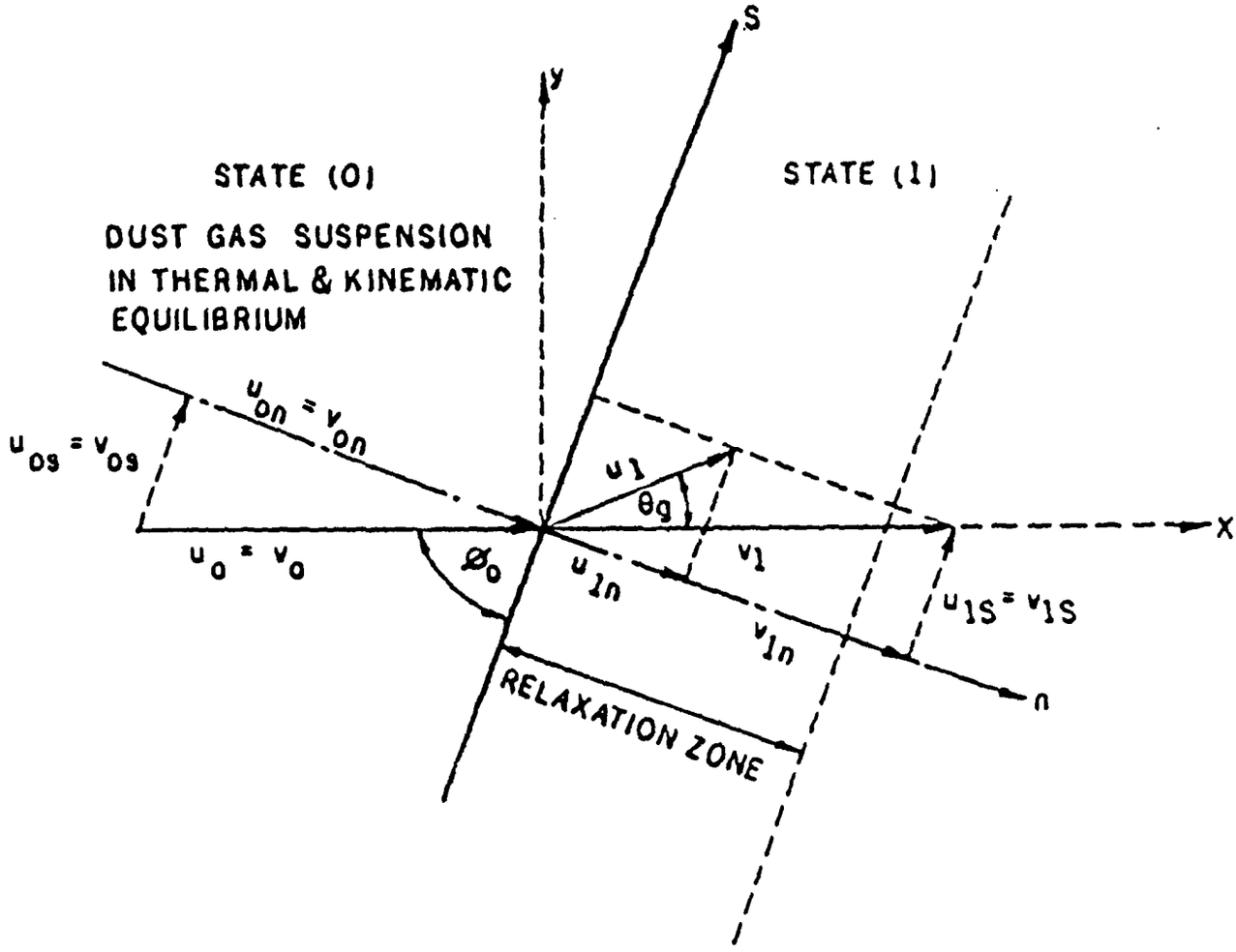

Figure 2: A schematical illustration of an oblique shock wave in a dusty gas and the definition of the (x,y)- and (n,s)-planes.

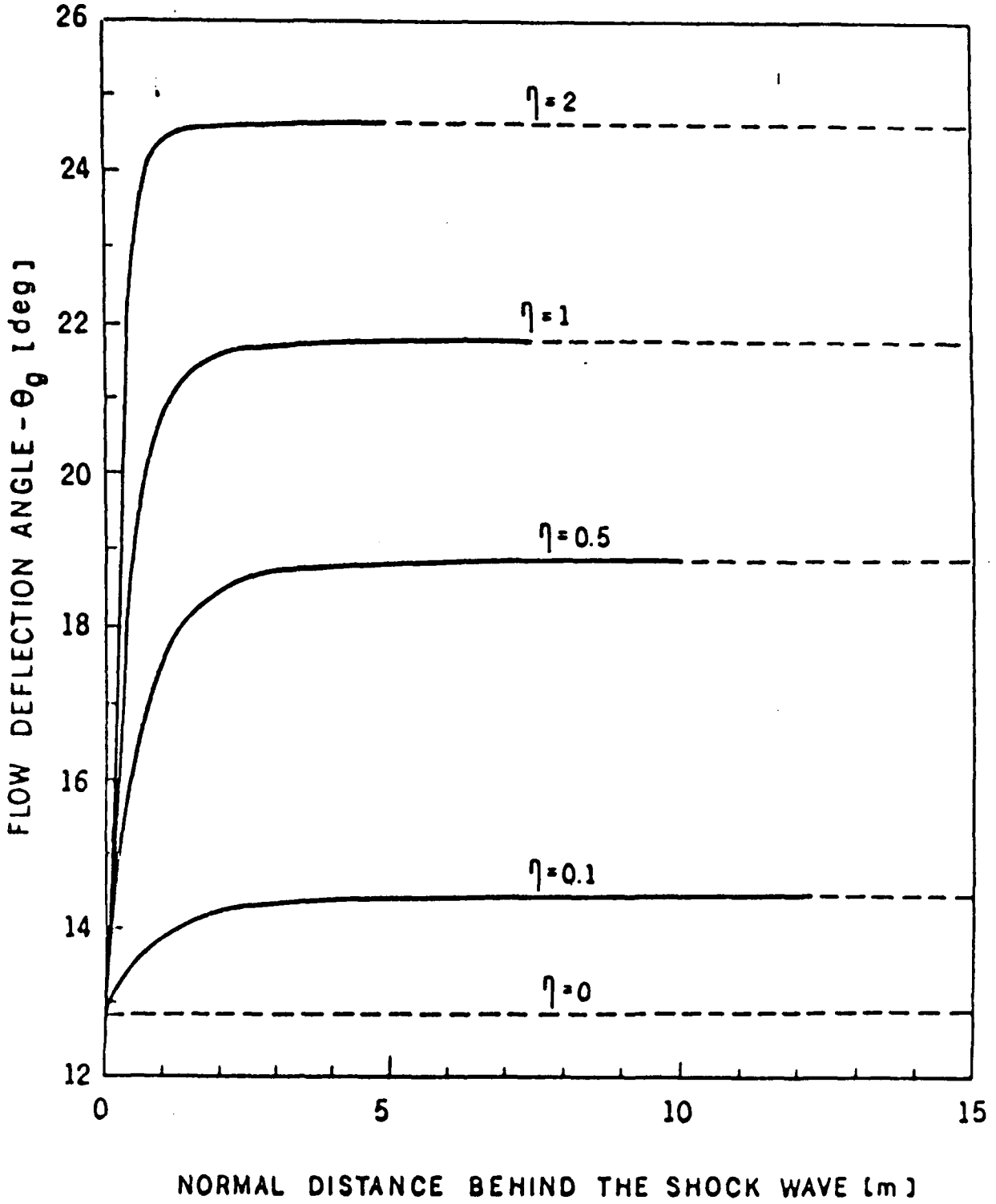

Figure 3: The change of the flow deflection angle θ_g with normal distance from the shock wave for various loading ratios η and $M_0 = 3$, $\phi = 30^0$, $D = 100\ \mu m$, and $C = 1000\ J/(Kgm\ K)$.

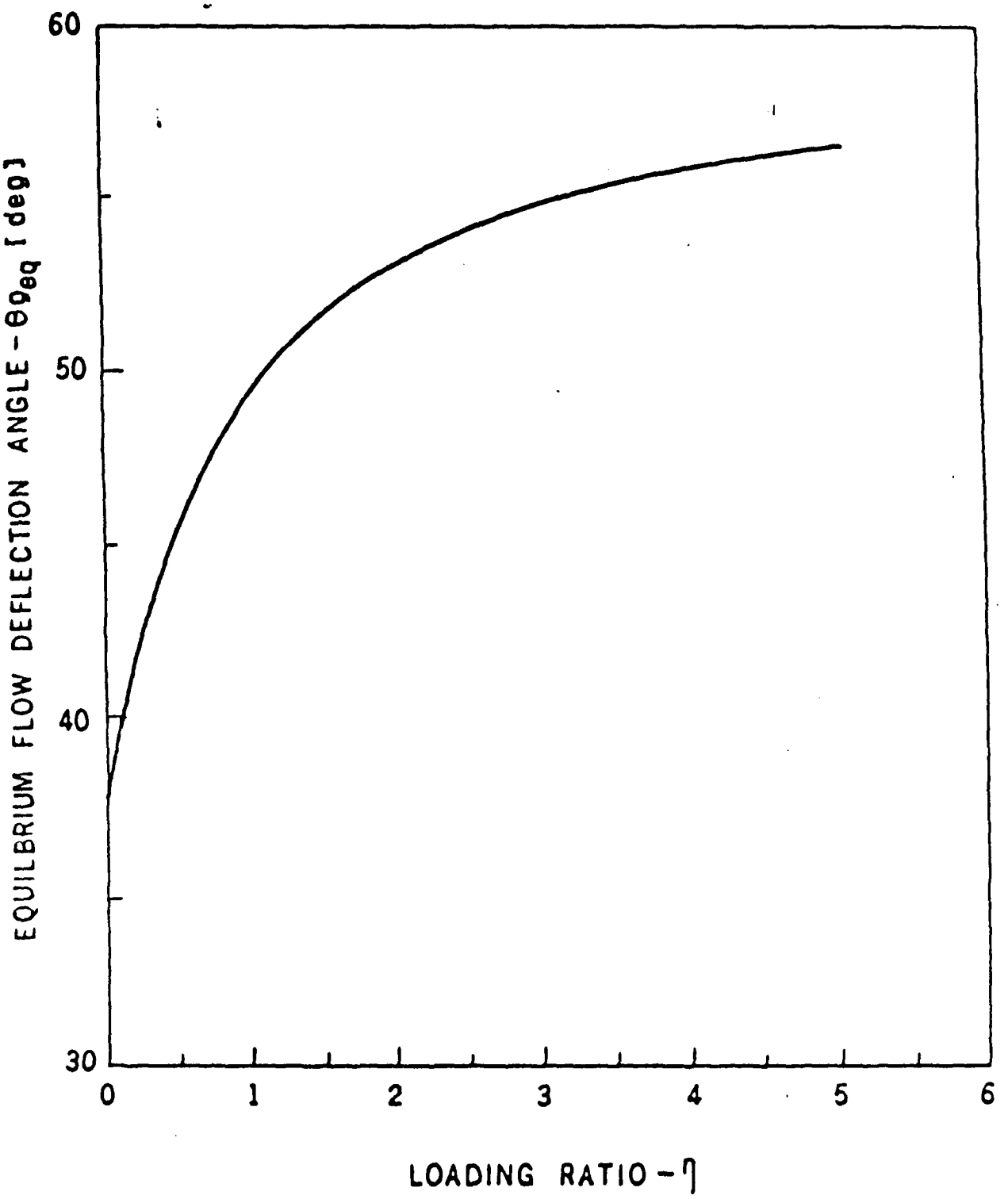

Figure 4: The equilibrium flow deflection angle, $\theta_{\theta_{eq}}$, as a function of the loading ratio, η, for $M_0 = 4$, $\phi = 60^0$, $D = 100\ \mu m$, and $C = 1000\ J/(Kgm\ K)$.

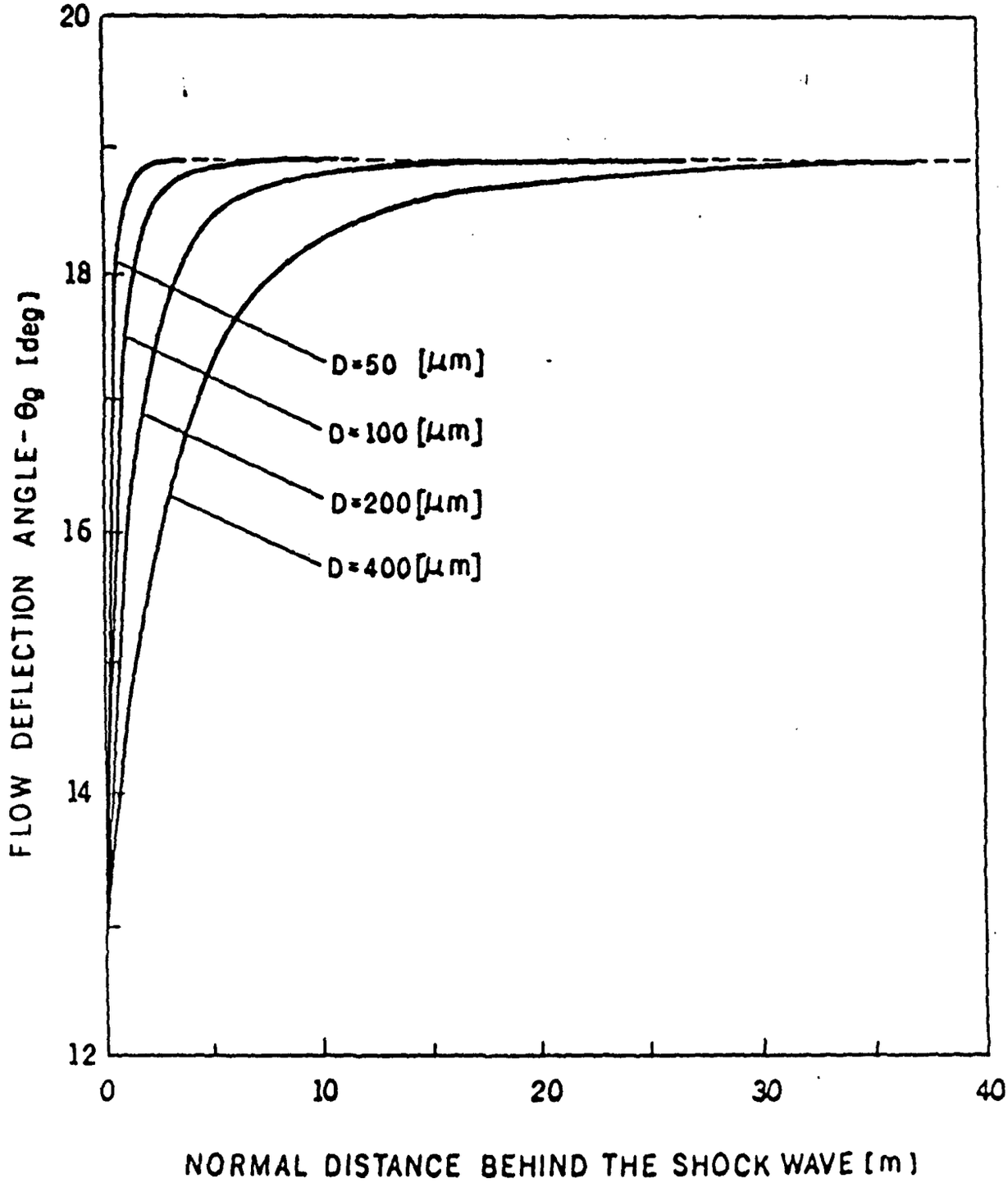

Figure 5: The change of the flow deflection angle with normal distance from the shock wave for various solid particle diameters, D, $M_0 = 3$, $C = 1000 J/(Kgm\ K)$, $\phi_0 = 30^0$, and $\eta = 0.5$.

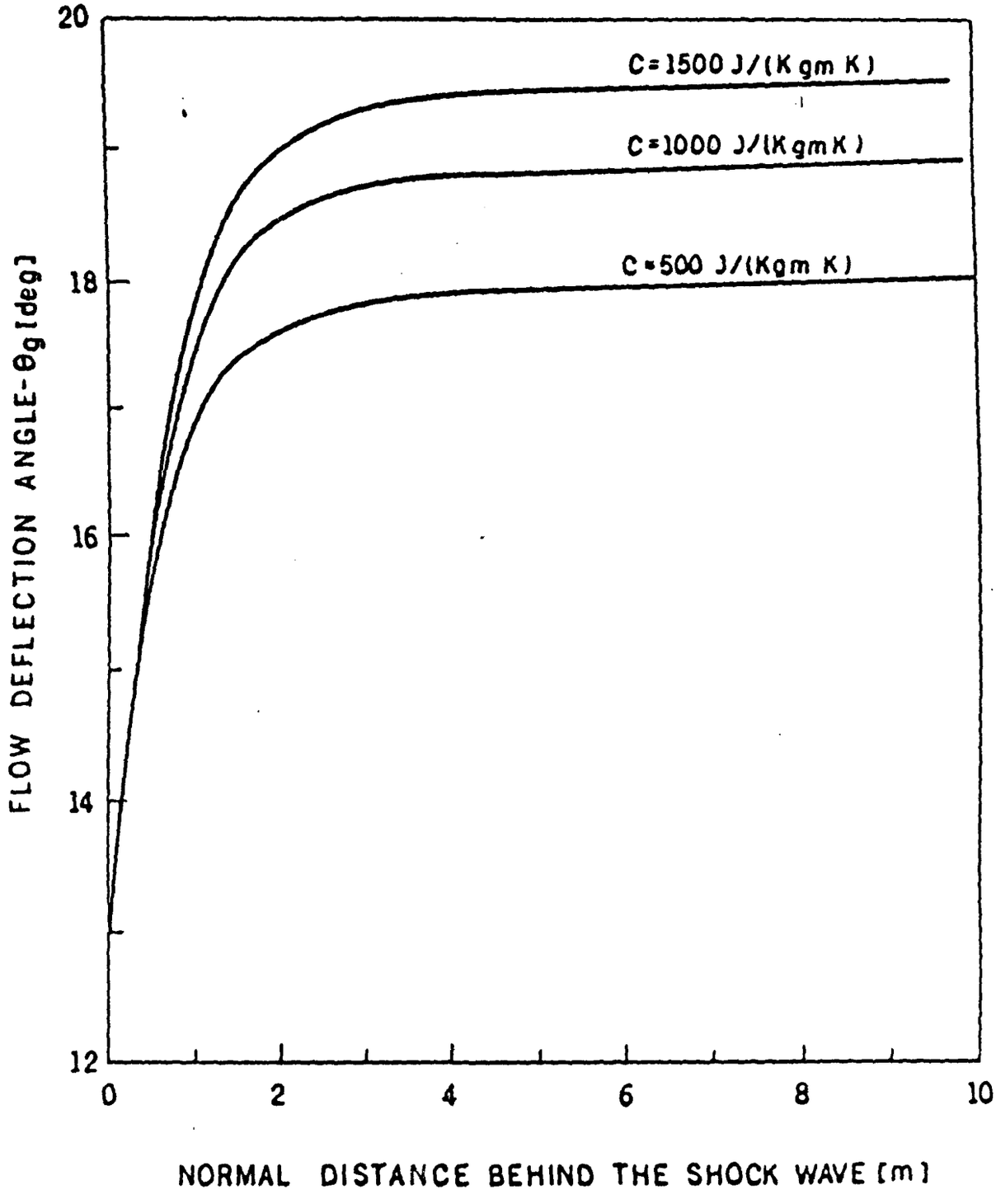

Figure 6: The change of the flow deflection angle with normal distance from the shock wave for various values of specific heat capacity of the solid particles, C, and $M_0 = 3$, $\phi_0 = 30^0$, $D = 100\ \mu m$, and $\eta = 0.5$.

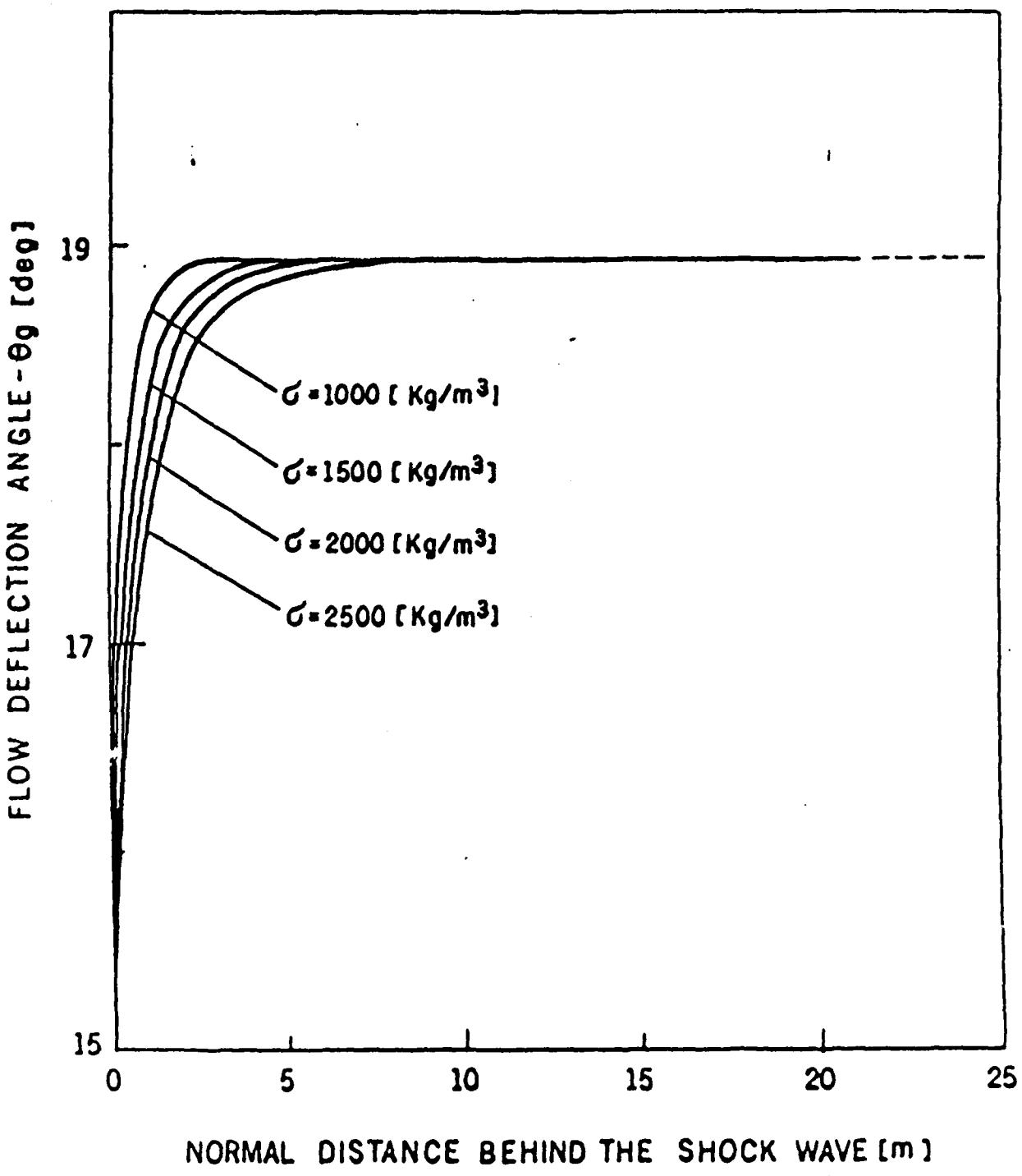

Figure 7: The change of the flow deflection angle with distance from the shock wave for various values of material density of the solid particles, σ, and $M_0 = 3$, $\phi_0 = 30^0$, $D = 100\ \mu m$, $C = 1000\ J/(Kgm\ K)$, and $\eta = 0.5$.

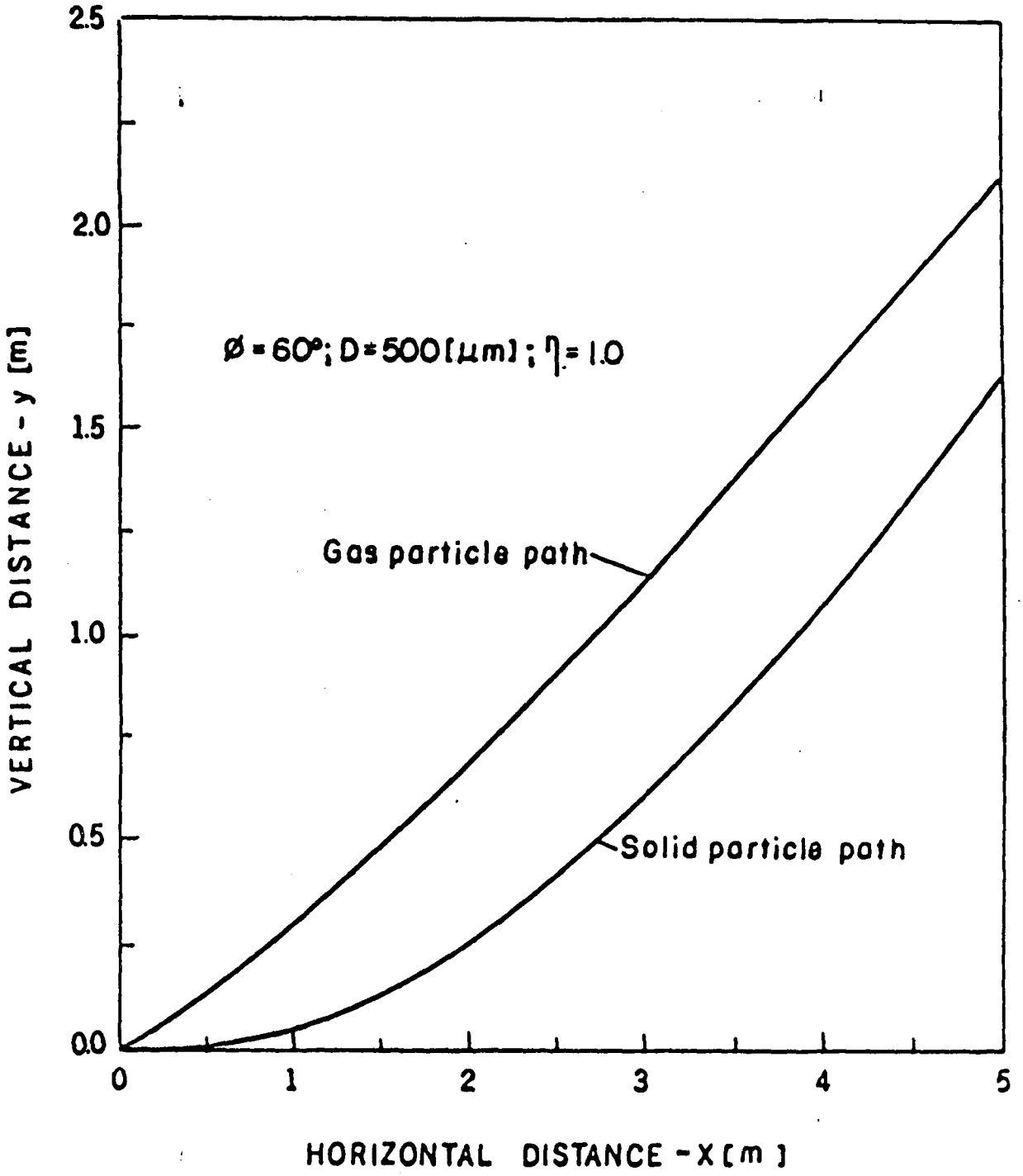

Figure 8: The gas and solid particles paths in the (x,y)-plane for $M_0 = 3$, $\phi_0 = 60^0$, D = 500 μm, C = 1000 J/(Kgm K), σ = 1000 Kgm/m^3, and $\eta = 1$.

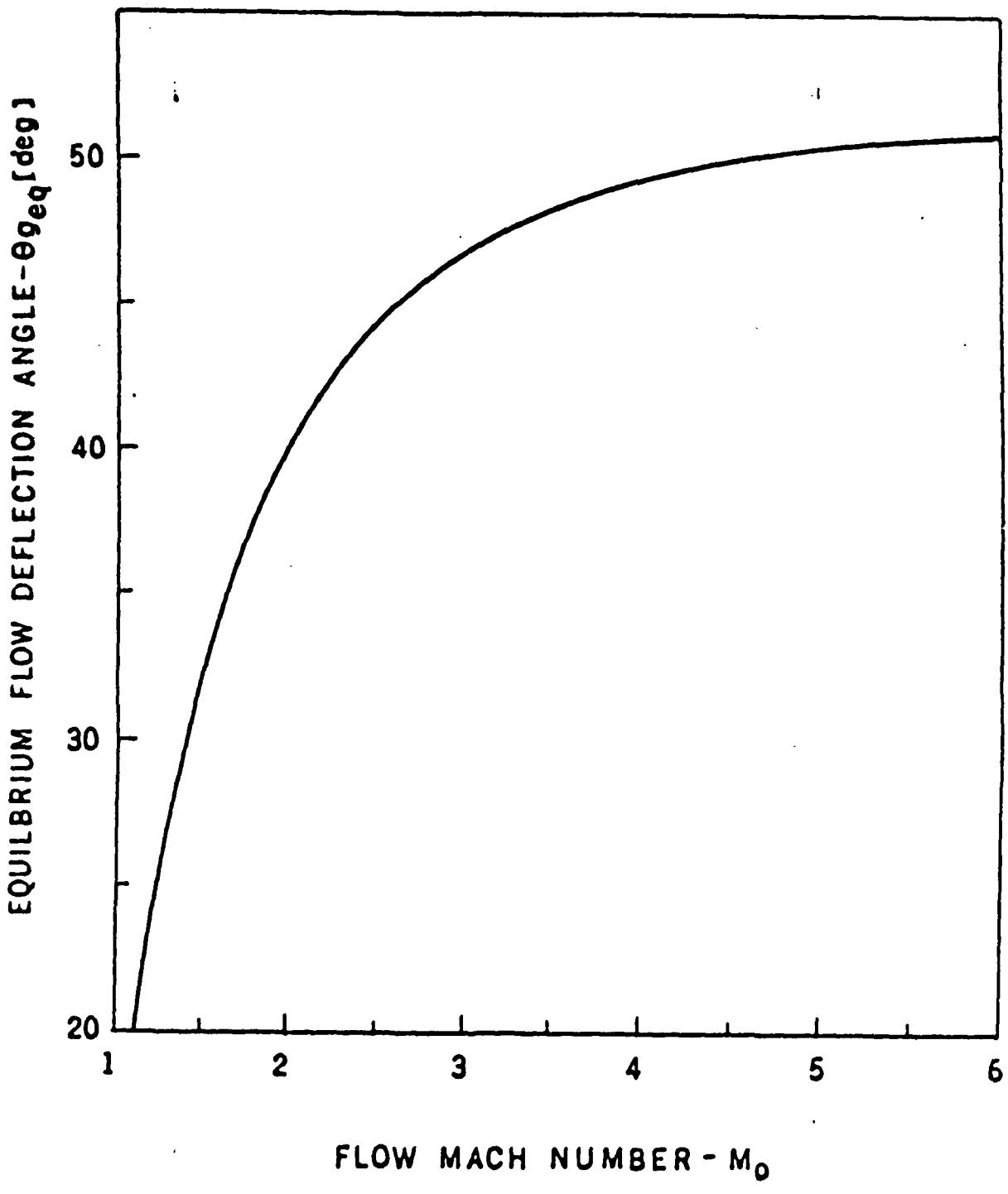

Figure 9: The dependence of the equilibrium flow deflection angle, θ_{eq}, on the incident flow Mach number, for $\phi = 60^0$, $D = 200\ \mu m$, $C = 1000\ J/(Kgm\ K)$, $\sigma = 1000\ Kgm/m^3$ and $\eta = 1$.

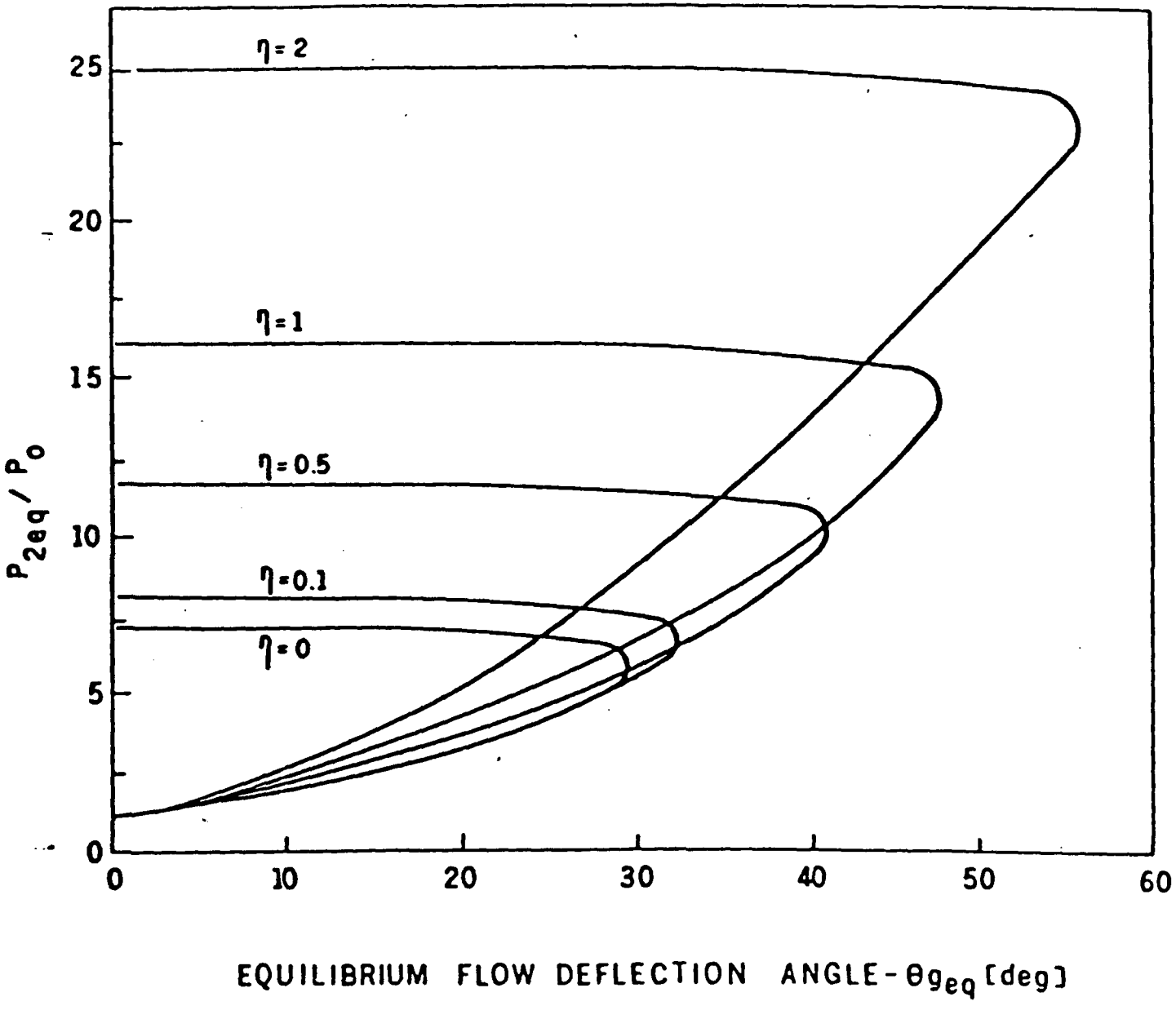

Figure 10: The (P, θ_g)-shock polar for $M_0 = 2.5$, $D = 100\ \mu m$, $C = 1000\ J/(Kgm\ K)$, $\sigma = 1000\ Kgm/m^3$, and different values of the loading ratio η.

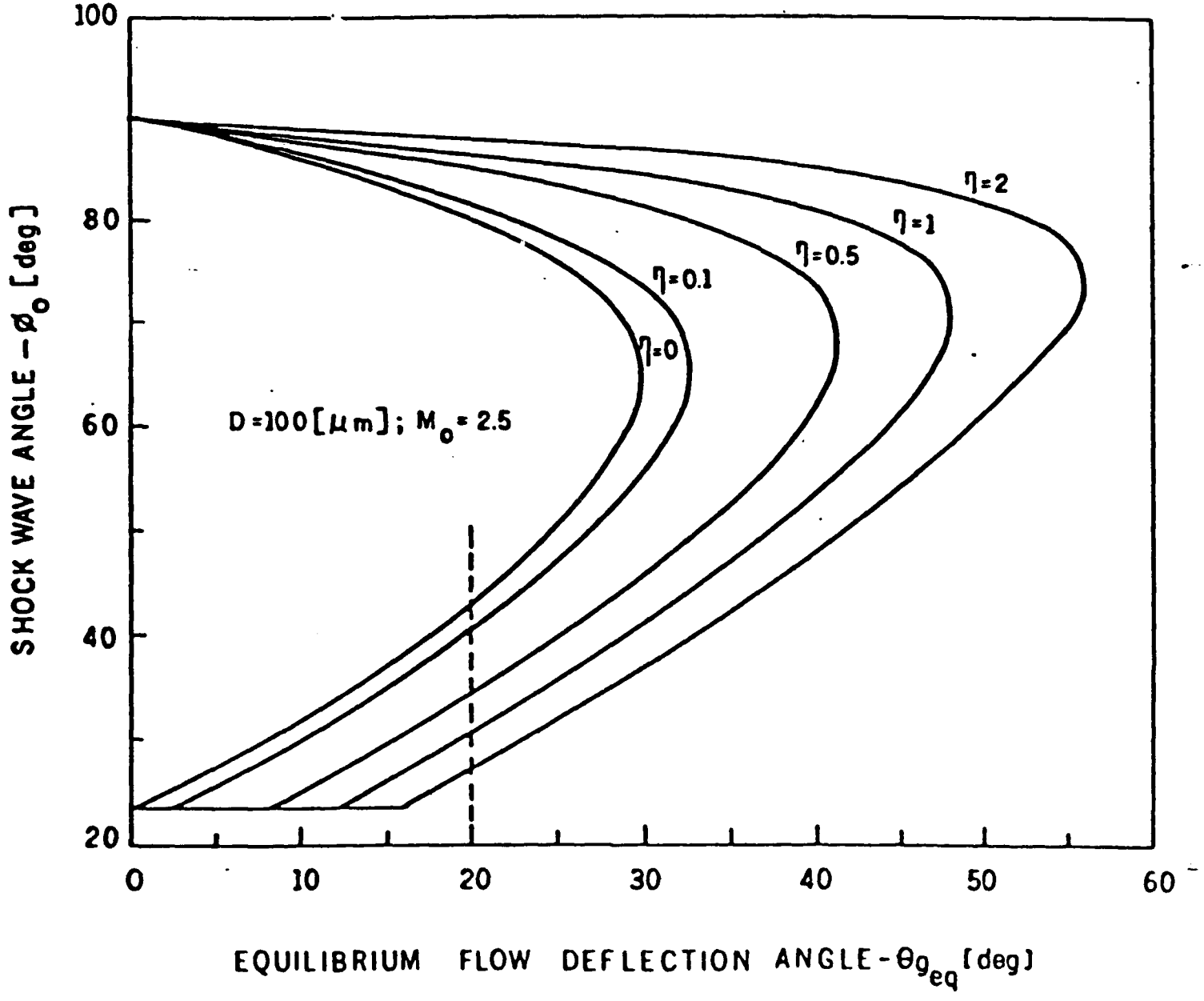

Figure 11: The (ϕ, θ_g)-shock polar for $M_0 = 2.5$, $D = 100\ \mu m$, $C = 1000\ J/(Kgm\ K)$, $\sigma = 1000\ Kgm/m^3$, and different values of the loading ratio η.

Part 2

The Flow of a Dust-Gas Suspension with Dust Having Various Distributions of its Physical Properties Through a Normal Shock Wave.

Abstract

The effect of distributions of non-uniformities in the diameter, heat capacity and material density of small spherical particles on the properties of a dust-gas suspension passing through a normal stationary shock wave is studied numerically.

It was found that the gas temperature is practically independent of the size distribution of the dust particles. The suspension pressure, however, is very sensitive to the size distribution. It rises very sharply when the suspension contains mainly small particles.

A distribution in the specific heat capacity of the solid particles results in a minor effect on the velocities and the pressure, and a pronounced effect on the temperature of the solid particles.

A distribution in the material density of the solid particles affects both the velocities and the temperatures of the solid and gaseous phases.

Introduction

The interest in the gas-dynamic behaviour of a gas-particle suspension grew in the past three decades due to its application in many engineering problems. Some typical examples are: metalized propellants of rockets, jet-type dust collectors and blast waves in dusty atmospheres. In addition, mixtures with gases heavily laden with particles occur frequently in industrial processes such as plastics manufacturing, flour milling, coal-dust conveying, powder metallurgy and powdered-food processing. General descriptions of such flows can be found in several books and review papers [Soo (1967), Marble (1970) and Rudinger (1973)]

The major differences between the flow fields which are developed behind a normal shock wave in a dusty-gas and a pure (dust-free) gas are illustrated in figures 1a and b for the temperatures and the velocities,

respectively. When a steady pure gas encounters a normal shock wave it experiences a sharp (almost discontinuous) change in its thermodynamic and kinematic properties. This sudden change is shown in figure 1 to occur between (0) and (1). The thickness of this disturbance, l_f, is only a few mean free paths of the gas atoms or molecules. Beyond (1) the gas properties remain constant (solid lines in figures 1a and b) provided the gas conditions at (1) are not sufficient to excite the internal degrees of freedom of the gas.

If, however, the gas is laden with solid particles then the suspension which was originally at a state of thermodynamic and kinematic equilibrium, ahead of the shock front, is suddenly changed into a non-equilibrium state, because the solid particles, due to their size compared with l_f, do not experience any noticeable change in their properties upon moving from (0) to (1). Thus, at (1) the gas has a much higher temperature than the dust, $T_g >> T_p$, and a much lower velocity, $u << v$ (u is the gas velocity and v is the velocity of the solid particles). Morgenthaler (1962) indicated that this is true even if the particle diameter is as small as 0.1 μm (for shock waves in air at nearly standard conditions, where the mean free path is about 0.066 μm). Therefore, the particles are not influenced by the initial disturbance, and the gas properties at (1) can be safely assumed to be identical to those of a pure gas with the same initial conditions.

Far downstream of (1), i.e., at (∞) in figure 1, the gas and the solid phases reach a new state of thermodynamic and kinematic equilibrium via momentum and energy exchange. Theoretically all shock waves in dusty gases are infinitely thick, since equilibrium is approached asymptotically. However, it is a common practice to assign to the shock wave an effective thickness which is defined by a requirement that the suspension properties come close to their equilibrium downstream values. It was shown by Gottlieb & Coskunses (1985) that the suspension equilibrium properties (at infinity) can be calculated from the usual normal shock wave relations, provided that the usual pure gas parameters γ and R (the specific heat capacities ratio and the specific gas constant) are replaced by effective values $\bar{\gamma}$ and $\bar{R}$ which solely depend on the initial conditions of the suspension. This effective thickness is known in the literature as the relaxation zone, for it is analogous to the relaxation zone in pure gases

where the internal degrees of freedom are excited. The extent of the relaxation zone strongly depends on the momentum and heat transfer mechanisms which enable the solid and the gaseous phases to reach a new equilibrium state. The analysis of the relaxation zone was studied by many investigators. The pioneering works of Carrier (1958), Kriebel (1964) and Rudinger (1964) verified the existence of this relaxation zone and identified the parameters affecting it, namely; the solid particle diameter, D, its heat capacity, C, its material density, σ, and the loading ratio, η. Igra & Ben-Dor (1980) compared various correlations for the drag coefficient, C_D, and the heat transfer coefficient, Nu, and pointed out their effect on the extent of the relaxation zone. In addition they studied the role of thermal radiation heat transfer between the two phases and showed that it can be neglected when the incident shock wave Mach number is smaller than five.

In all the above mentioned works, as well as in many others, the gaseous phase was assumed to behave as a perfect gas. This assumption was recently relaxed by Ben-Dor & Igra (1982) and Igra & Ben-Dor (1984) who solved the flow field while accounting for real gas effects. Dissociating nitrogen was the gaseous phase in the latter work and ionizing argon in the former.

The assumption that the solid particles are inert, which was also adopted in most of the published studies, was also relaxed by Elperin, Ben-Dor & Igra (1986) who solved the flow field of an oxygen-carbon suspension passing through a normal shock wave, behind which the carbon particles reached their ignition temperature and burned out.

In the present study, another commonly used assumption concerning the solid phase is relaxed. It has been a common practice to assume that the solid phase consists of spherical particles of identical diameter, D, identical material density, σ, and heat capacity, C. In reality, however, this is not the case, for the particles comprising the solid phase do not have, in general, a uniform size even though they might have the same physical properties, i.e., σ and C. Furthermore, there could be cases in which the suspension consists of different solid materials, i.e., σ and C.

The purpose of this study is to numerically investigate the influence of the above mentioned solid phase non-uniformities on the flow field which is developed behind a normal shock wave.

In the following, the basic assumptions upon which the present model is based are given. The assumptions are followed by the governing equations and the numerical results arising from their solution.

Theoretical Background

Assumptions

The assumptions upon which the present model is based and their implications are listed in the following:

1) The gaseous phase behaves as an ideal gas. Thus, the equation of state of the gas is $P = \rho_g R T_g$. Note that it is not assumed here that the gas is calorically ideal. Alternatively, the dependence of both C_p and C_v on the gas temperature is accounted for. This has not been done in previous studies where both C_p and C_v were assumed to be constant.
2) All solid particles are rigid, chemically inert small spheres uniformly distributed in the gaseous phase. Thus there is no heat addition or reduction due to chemical processes between the solid and the gaseous phases. Furthermore, Re and Nu are based on the particle diameter, D.
3) The volume of the solid phase in the suspension can be neglected. Thus the momentum and energy exchange between the solid particles can be ignored.
4) Aside from momentum and energy interactions between the gaseous and the solid phases, the gaseous phase is considered to be a perfect fluid, i.e., no other viscous or conduction effects are considered.
5) The solid particles are too large to experience any change in their thermodynamic and dynamic properties upon their passage through the shock front. In addition they are also large enough not to experience Brownian motion. Thus, the partial pressure of the solid phase can be neglected.
6) The solid particles are small enough to satisfy the condition $B_i < 0.1$, where B_i is the Biot number, $B_i = hr/k_p$ (h is the coefficient of heat transfer, r is the radius of the particle, and k_p is its thermal conductivity). Thus the temperature within the solid particles can be assumed to be uniform.

7) The weight of the solid particles and the buoyancy forces experienced by them are negligibly small in comparison with the drag forces acting on them.
8) The heat capacity, C, of the solid particles is constant.
9) Ahead of the normal shock wave the suspension is at a state of thermodynamic and dynamic equilibrium, i.e., $u_0 = v_0$ and $T_{g0} = T_{p0}$, where u and v are the velocities of the gas and the solid particles, and T_g and T_p are the temperatures of the gas and solid particles, respectively.

In addition to the above listed assumptions it is assumed that the flow field under consideration is one-dimensional and steady.

Governing Equations

Prior to listing the governing equations it should be mentioned that the considered suspension is composed of n + 1 phases. One phase is the gaseous phase. The remaining n phases are all solid phases. Each of the n solid phases consists of identical particles. However, each one of the n solid phases differ from all the other solid phases in, at least, one of the following properties; the diameter of the solid particle, D, its material density, σ, or its heat capacity, C.

Based on the foregoing assumptions the governing equations describing the problem at hand are:

- continuity of the gaseous phase;

$$\frac{d}{dx}(\rho_g u) = 0 \qquad (1)$$

- continuity of the i-th solid phase;

$$\frac{d}{dx}(\rho_{pi} v_i) = 0 \qquad i = 1 \text{ to } n \qquad (2)$$

- conservation of momentum of the gaseous phase;

$$\frac{d}{dx}(\rho_g u^2 + P) = \sum_1^n F_{Di} \qquad (3)$$

- conservation of momentum of the i-th solid phase;

$$\frac{d}{dx}(\rho_{pi} v_i^2) = -F_{Di} \qquad (4)$$

- conservation of energy of the gaseous phase;

$$\rho_g u \frac{d}{dx}[C_p T_g + 1/2\, u^2] = \sum_1^n Q_{pi} + \sum_1^n F_{Di} v_i \qquad (5)$$

- conservation of energy of the i-th solid phase;

$$\rho_{pi} v_i \frac{d}{dx}[C_i T_{pi} + 1/2\, v_i^2] = -Q_{pi} - F_{Di} v_i \qquad (6)$$

- equation of state of the gaseous phase;

$$P = \rho_g R T_g \qquad (7)$$

In the above equations ρ_g, u, T_g and P are the density, velocity, temperature and pressure of the gaseous phase, respectively, ρ_{pi}, v_i and T_{pi} are the spatial density, velocity and temperature of the i-th solid phase, respectively. Note that the material density of the solid particles is σ_i which can be related to the spatial density ρ_{pi} via the relation $\rho_{pi} = n_i V_{pi} \sigma_i$ where n_i is the number density of the i-th solid particle and V_{pi} is the volume of a single i-th solid particle. It should also be noted that according to assumption 5 the partial pressures of all the solid phases are zero. For this reason P is not only the pressure of the the gaseous phase, but the pressure of the suspension as well. C_p and R are the specific heat capacity at constant pressure and the specific gas constant of the gaseous phase and C_i is the heat capacity of the particles of the i-th solid phase. F_{Di} is the

drag force per unit volume exerted by the gaseous phase on the particles of the i-th solid phase and Q_{pi} is the heat transferred per unit volume from the particles of the i-th solid phase to the gaseous phase.

The drag force F_{Di} can be calculated from:

$$F_{Di} = 3/4\ \rho_g \rho_{pi}\ (v_i - u)\ |\ v_i - u\ |\ C_{D_i} / (D_i\ \sigma_i) \qquad (8)$$

where D_i is the diameter of the solid particle, σ_i is their material density, and C_{D_i} the drag coefficient is given by

$$C_{D_i} = 0.48 + 28\ Re_i^{-0.85} \qquad (9)$$

The slip Re number for the i-th solid phase is given by

$$Re_i = \frac{\rho_g |v_i - u\ | D_i}{\mu_g} \qquad (10)$$

where the dynamic viscosity, μ_g, depends on the gas temperature, T_g.

The transferred heat, Q_{pi}, can be calculated from:

$$Q_{pi} = 6h_i\ \rho_{pi}\ (T_{pi} - T_g) / (D_i\ \sigma_i) \qquad (11)$$

where h_i, the coefficient of convection heat transfer can be obtained from

$$h_i = \frac{k_g Nu_i}{D_i} \qquad (12)$$

Nu_i is the Nusselt number of the i-th solid phase. It can be obtained from

$$Nu_i = 2 + 0.459\ Pr^{0.33}\ Re_i^{0.55} \qquad (13)$$

In the last expression Pr is the Prandtl number;

$$Pr = \frac{\mu_g C_p}{k_g} \qquad (14)$$

where k_g (also in 12) is the thermal conductivity of the gaseous phase.

The above set of governing equations consists of 4 + 3n equations (conservation of mass, momentum and energy for the gaseous phase, equation of state of the gaseous phase and conservation of mass, momentum and energy for each of the n solid particles). The number of the unknowns in the above set of equations is also 4+3n (ρ_g, u, T_g and P for the gaseous phase and ρ_{pi}, v_i and T_{pi} for each of the n solid phases). Thus the above set of governing equations is solvable in principle.

Numerical Approach

Computer Code

There are many computational packages capable of numerically solving differential equations. The one chosen for solving the differential equations governing the problem at hand is the IMSL (International Mathematical & Statistical Libraries) package suited to operate on a CDC Cyber 840 computer. The IMSL package contains three computer codes for solving differential equations with given initial conditions; they are:

DVERK - based on the Runge-Kutta method, and recommended for cases where high accuracy is not required and where the derivatives can be simply calculated.

DGEAR - based on the predictor-corrector method. Although it results in poor accuracy it is preferable to DVERK when the calculation of the derivatives is difficult and hence expensive.

DREBS - based on the extrapolation method. Preferable when high accuracies are required and when the derivatives can be calculated in a relatively simple and inexpensive way.

The DREBS code was adopted in the present study because it is the most accurate one. This code performs a triple check of the obtained error between each two extrapolation steps. Since the DREBS code is limited to the case where each derivative is independent of the other derivatives the governing equations need to be rearranged. The rearrangement of the governing equations (1) to (7) results in;

$$\frac{dT_g}{dx} = \frac{\sum\left(Q_{pi} + F_{Di}v_i - \frac{F_{Di}\,u^3}{u^2-RT_g}\right)}{\rho_g u\left(C_p - \frac{Ru^2}{u^2-RT_g}\right)} \qquad (15)$$

$$\frac{du}{dx} = \frac{\Sigma F_{Di} - \rho_g R \frac{dT_g}{dx}}{\rho_g \frac{u - RT_g}{u}} \qquad (16)$$

$$\frac{dP}{dx} = \rho_g R \left(\frac{dT_g}{dx} - \frac{T_g}{u} \frac{du}{dx} \right) \qquad (17)$$

$$\frac{d\rho_g}{dx} = \frac{\rho_g}{u} \frac{du}{dx} \qquad (18)$$

$$\frac{dT_{pi}}{dx} = \frac{Q_{pi}}{C_i \rho_{pi} v_i} \qquad (19)$$

$$\frac{dv_i}{dx} = \frac{F_{Di}}{\rho_{pi} v_i} \qquad (20)$$

$$\frac{d\rho_{pi}}{dx} = \frac{\rho_{pi}}{v_i} \frac{dv_i}{dx} \qquad (21)$$

Note that although equations (15) to (21) do not reflect the dependence of the gas specific heat capacity on its temperature since a space gradient of C_p does not appear, the value of C_p was calculated at any position x according to the temperature of that position. This procedure assumes that the space gradient of C_p is neglectable.

Initial Conditions

As mentioned earlier the properties of the solid phases do not change when they pass through the normal shock wave. Thus, the solid particles velocity, v_i, temperature T_{pi}, and spatial density, ρ_{pi}, immediately behind the shock front remain identical to their appropriate values ahead of the shock front, i.e.,

$$(v_i)_1 = (v_i)_0$$
$$(T_{pi})_1 = (T_{pi})_0$$
$$(\rho_{pi})_1 = (\rho_{pi})_0$$

Furthermore, the multi-phase suspension is assumed to be in thermodynamic and kinematic equilibrium ahead of the shock front,

therefore; $(v_i)_0 = u_0$ and $(T_{pi})_0 = T_0$ and $(\rho_{pi})_0 = \eta_i \rho_{g_0}$ where η_i is the loading ratio of the i-th solid phase.

The properties of the gas, on the other hand, change almost discontinuously across the shock wave. The gas properties, immediately behind the shock front, can simply be calculated from the normal shock jump conditions, i.e.,

$$\frac{P_1}{P_0} = \frac{2\gamma M_0^2}{\gamma+1} - \frac{\gamma-1}{\gamma+1} \qquad (23)?$$

$$\frac{\rho_{g_1}}{\rho_{g_0}} = \frac{(\gamma+1)M_0^2}{(\gamma-1)M_0^2+2} \qquad (24)$$

$$\frac{T_{g_1}}{T_{g_0}} = \frac{\left(1+\frac{\gamma-1}{2}M_0^2\right)\left(\frac{2\gamma}{\gamma-1}M_0^2-1\right)}{M_0^2\,\frac{(\gamma+1)^2}{2(\gamma-1)}} \qquad (25)$$

$$M_1 = \frac{M_0^2 + \frac{2}{\gamma-1}}{\frac{2\gamma}{\gamma-1}M_0^2-1} \qquad (26)$$

$$u_1 = M_1\sqrt{\gamma R T_{g_1}} \qquad (27)$$

M_0 and M_1 in the above equations are the flow Mach numbers immediately ahead and behind the shock front.

The Final Conditions

As mentioned the extent of the relaxation zone in the case of a dusty gas is infinitely long for the equilibrium values are approached asymptotically. However, as shown by Gottlieb & Coskunses (1985) the suspension equilibrium properties at infinity can be calculated very simply by using the above listed normal shock wave equations [(23) to (27)] and

replacing γ by $\bar{\gamma}$ and R by $\bar{R}$. In this approach the multi-phase suspension is assumed to be a single phase gas having new values for γ and R. Based on Gottlieb & Coskunses (1985), the relations for $\bar{\gamma}$ and $\bar{R}$ are as follows:

$$\bar{\gamma} = \frac{\Sigma\eta_i C_i + (1-\Sigma\eta_i)Cp}{\Sigma\eta_i C_i + (1-\Sigma\eta_i)Cv} \tag{28}$$

$$\bar{R} = (1-\Sigma\eta_i)R \tag{29}$$

where

$$\eta_i = \frac{\rho_{pi}}{\Sigma\rho_{pi} + \rho_g} \tag{30}$$

Note that in many papers the loading ratio is defined as $\eta_i^* = \rho_{pi}/\rho_g$. Thus, the two different definitions can be related by the following expression:

$$\eta_i = \frac{\eta_i^*}{\Sigma\eta_i^* + 1} \tag{31}$$

(It is clear from these relations that if the total loading ratio $\Sigma\eta_i$ and heat capacity C_i are constant, then $\bar{\gamma}$ and $\bar{R}$ are constant and hence the equilibrium properties at the end of the relaxation zone are identical.) These new values, i.e., $\bar{\gamma}$ and $\bar{R}$ yield a new speed of sound $\bar{a}$, which satisfies;

$$\bar{a}_0 < a_0 = (\gamma R T_{g_0})^{1/2}$$

Thus the flow Mach number ahead of the shock wave becomes $\bar{M}_0 > M_0$. By replacing γ, R and M_0 in equations (23) to (27) with $\bar{\gamma}$, $\bar{R}$ and $\bar{M}_0$, one can calculate the equilibrium properties of the suspension at infinity.

The knowledge of the suspension properties at infinity, i.e., the equilibrium final conditions can serve as an excellent means of checking the

reliability of the numerical results since they should be approached asymptotically.

Since the equilibrium conditions at infinity are known apriori the integration was terminated when the suspension properties came as close as 2% of their corresponding equilibrium value. The distance where the velocities reached this condition is called the kinematic relaxation length, l_v, and the distance where the temperatures reached this condition is called the thermal relaxation length, l_T. These two relaxation lengths are in general different.

Physical Properties of the Various Phases

The gaseous phase was chosen to be nitrogen. Yum, Weissman & Mason (1962) have calculated the transport properties of nitrogen and presented their results in a tabular form for both the dynamic viscosity, μ_g, and the thermal conductivity, k_g. A least square polynomial fit to their results yields the following expressions for k_g and μ_g;

$$k_g[W/(mK)] = 1.386 \times 10^{-2} + 5.311 \times 10^{-5} T_g - 9.822 \times 10^{-10} T_g^2$$

and

$$\mu_g[Kgm/(m\ sec)] = 0.7226 \times 10^{-5} + 2.768 \times 10^{-8} T_g - 0.5933 \times 10^{-12} T_g^2$$

The expression for the specific heat capacity at constant pressure, C_p, was adopted from Sontag & Van-Wylen (1971);

$$C_p[m^2/(sec^2\ K)] = 1.3686 \times 10^3 - 2.786 \times 10^5 T_g^{-1} + 5.1741 \times 10^7 T_g^{-2}$$

In the above expression T_g is in degree K.

Five solid phases were chosen in order to numerically simulate the effect of non-uniformities of the solid particles on the flow field. Thus, in equations (18) and (20) n = 5 and each of equations (15) to (17) represents five equations with i = 1, 2, ..., 5.

Each solid phase is identified by three parameters. The diameter of its particles, D_i, the heat capacity of its particles C_i and their material density, σ_i.

Nine different cases (for $M_0 = 1.5$) were investigated. They are shown in tables 1 to 3. In table 1 all the five solid phases have the same material density $\sigma_1 = \sigma_2 = \ldots = \sigma_5 = \sigma$ and heat capacity $C_1 = C_2 = \ldots = C_5 = C$ but different particle diameters $D_1 = 5\mu m$, $D_2 = 7.5\mu m$, $D_3 = 10\mu m$, $D_4 = 25\mu m$ and $D_5 = 50\mu m$. The seven cases differ in the loading ratios of the various solid phases.

The partial loading ratios η_i are chosen in such a way that the total loading ratios for each case, i.e, $\eta_{total} = \sum_{1}^{5} \eta_i$ equals always 0.2.

Thus, for all the seven cases, the suspension properties should reach the same equilibrium values at the end of the relaxation zone.

In the case shown in table 2 also for $M_0 = 1.5$, the five solid phases have identical particle diameters, $D = 50\mu m$ and material densities, $\sigma = 1500$ Kgm/m^3, but different heat capacities $C_1 = 100$, $C_2 = 500$, $C_3 = 1000$, $C_4 = 5{,}000$ and $C_5 = 10000$ J/(Kgm K). The loading ratio of each solid phase is $\eta = 0.04$ and therefore the total loading ratio is again 0.2.

The last case is shown in table 3. Here all the solid phases have identical particle diameters, $D = 10\mu m$ and heat capacities, $C = 1000$ J/(Kgm K), but different material densities, $\sigma_1 = 1000$, $\sigma_2 = 1250$, $\sigma_3 = 1500$, $\sigma_4 = 1750$ and $\sigma_5 = 2000$ Kgm/m^3. The incident shock wave Mach number is again $M_0 = 1.5$ and the total loading ratio is 0.2 ($\eta_i = 0.04$ for each solid phase).

Numerical Results and Discussions

Distribution of the Diameter of the Dust Particles

Figures 2 to 7 illustrate the flow field properties which are developed behind a normal shock wave with $M_0 = 1.5$ in cases 1 to 6, respectively (see table 1). Each of these six figures contains six velocity and six temperature profiles (one for the gaseous phase labelled with "G" and five for each of the five solid phases labelled "1" to "5" in accordance with table 1) and one pressure profile. The dashed lines in the right hand sides of figures 2 to 7 indicate the equilibrium values at infinity, which should be approached asymptotically. As mentioned earlier these values are calculated apriori.

It is clear from figures 2 to 7 that the larger the particle diameter is, the longer it takes for it to reach a dynamic equilibrium. This is due to the fact that the inertial forces depend on D_1^3 while the drag forces are roughly proportional to D_1^2. Thus the effectiveness of the drag forces in slowing down the solid particles decreases as the diameter of the solid particles increases. The solid phase with the larger particles is also the last to reach thermal equilibrium with the gaseous phase. This is not surprising since the larger the solid particle is, the slower will be its temperature rise. Thus the solid phase with the smallest particles (D = 5μm) reaches a thermal equilibrium with the gaseous phase within few centimeters while it takes tens of centimeters for the solid phase with the largest particles.

The velocity, temperature and pressure profiles of the gaseous phase for cases 1 to 6 are shown in figure 8. It is clearly seen in figure 8 that all the six cases approach asymptotically, identical equilibrium properties at infinity. This fact should not be surprising for the total loading ratio in all the six cases is $\eta = 0.2$ and the heat capacity of the solid particles is the same. Although the equilibrium properties are identical, the flow properties inside the relaxation zone do depend on the size distribution of the particles of each solid phase. The dependence is minimal for the gas temperature where the six profiles merge into an almost one curve, and it is maximal for the suspension pressure. The suspension pressure increases very sharply when it consists mainly of small particles (case 5) and it increases very slowly when it consists mainly of large particles (case 6). Thus it can be concluded that increasing the mass fraction of the small solid particles in the suspension results in a faster rise in the suspension pressure. Similarly, the suspension with the largest amount of small particles results in the sharpest decrease in the gaseous phase velocity. The suspension with the largest amount of large particles, experiences the smallest decrease in the gaseous phase velocity. It is interesting to note that the gaseous phase velocity falls from its value immediately behind the shock front in spite of the fact that it exchanges momentum with the solid phases which have much higher post shock velocities. The reason for this peculiar behaviour lies in the fact that the dust presence causes a very large increase in the density of the gaseous phase. This in turn results in a

large decrease in the gaseous phase velocity since the flow field is one dimensional and $\rho_g u$ must remain constant.

The general shapes of the various property profiles, for the six cases of multi-solid-phases, are similar to those obtained when the suspension contains a single-solid-phase only, i.e., case 7 in table 1, whose solution is seen in figure 9. Since for this case $\eta = 0.2$ too, the equilibrium properties at infinity are identical to those shown in figures 2 to 7.

The thermal and kinematic relaxation lengths for cases 1 to 7 are given in table 4. The earlier remark that the temperature of the gaseous phase is almost unaffected by the size distribution of the particles of the solid phases (see figure 8, where all the temperature profiles merge into a single line at a very short distance behind the shock fronts) is further supported by the fact that the thermal relaxation length l_T is almost the same for the six multi-phase cases.

The difference between the kinematic relaxation lengths, l_V, is much larger. The two extreme cases, 5 & 6, differ by about 8.5%. Note that the difference in the thermal relaxation length between the two extreme cases is only about 1.5%.

However, the difference in both the thermal and kinematic relaxation lengths between the multi-solid phases (case 1 to 6) and the single-solid phase (case 7) is enormous. Both l_T and l_V are more than 90% smaller when the suspension contains a single solid phase with $D = 10\mu m$. It is obvious that the enormous increase in both l_T and l_V when the suspension contains a size distributed solid phase arises from the presence of the large particles, $D = 50\mu m$, in the six cases. This is due to the fact that the large particles slow down and heat up very slowly in comparison with smaller particles. Thus it can be concluded that the extent of the relaxation zone is determined solely by the solid particle having the largest diameter.

Distribution of the Heat Capacity of the Dust Particles

Case 8 (table 2) in which the solid particles of the five phases have identical diameters $D = 50\mu m$ and material density $\sigma = 1500$ Kgm/m^3 but different heat capacities, C, were solved. The results are shown in figure 10 for $M_0 = 1.5$.

It is evident from figure 10 that in spite of the fact that the heat capacity, C, of each of the solid phases is different, they all have the same

velocity and pressure inside the relaxation zone. Thus, the heat capacity has no affect on the velocities of the solid particles and the gaseous phases and does not affect the suspension pressure. However, the five solid phases have different temperature profiles. The temperature of the solid particles with the highest value of C experiences the slowest increase. For the smallest value of C the temperature rise of the solid particles is extremely sharp. It overshoots the temperature of the gaseous phase before it drops down to the equilibrium value at infinity.

The thermal and kinematic relaxation lengths, l_T and l_V, are also shown in table 4 for this case (case 8). The large values for l_T arise from the fact that it takes a long time for the solid phase with the largest heat capacity to reach equilibrium with the gaseous phase because their temperature rise is very slow. The large values for the kinematic relaxation length are due to the fact that the diameter of all the solid particles was chosen to be D = 50μm for this case.

Distribution of the Material Density of the Dust Particles

Case 9 (table 3) in which the solid particles of the five phases have identical diameters D = 10μm and heat capacities C = 1000 J''Kgm K) but different material densities is shown in figure 11 for M_0 = 1.5. Case 7 which has identical values of D and C, as well as the total loading ratios of η = 0.2, but a constant value of σ = 1500 Kgm/m^3 is added to figure 11 in dashed lines.

The solid lines in figure 11 indicate that the distribution in the solid particles density results in a decrease in the gas pressure, temperature and velocity gradients behind the shock front. The equilibrium values, however, at infinity are identical for the two cases. In addition it is evident from figure 11 that the larger the material density of the dust particles is, the slower its decay becomes. This is so because its inertia depends linearly on the material density. Similarly, the larger the material density of the dust is, the slower its temperature rise becomes, because it has a higher heat capacity. The effect of the distribution in the material density of the dust particles on the thermal and kinematic relaxation lengths, l_T and l_V, respectively, can be seen by comparing cases 7 & 9 in table 4. For the M_0 = 1.5 case (7 & 9) both l_T and l_V increase by about 25%.

Conclusions

The flow field which is developed behind a steady normal shock wave in a dust-gas suspension has been solved numerically while accounting for distributions of non-uniformities in the physical properties of the solid phase. The model was based on a multi-phase system which consists of one gaseous phase and five solid phases. The five solid phases differed from each other by one physical property only, which was either the diameter of the solid particles or their heat capacity or their material density.

For a fixed total loading ratio it was found that the gas temperature profile downstream of the shock wave is practically independent of the size distribution of the dust particles. This might also be a result of the relatively small loading ratio which was used in the calculation. Consequently, it should not necessarily hold for an arbitrary loading ratio. The suspension pressure profile, however, is very sensitive to the size distribution. The suspension pressure rises very sharply when the suspension contains mostly small particles. Similarly the suspension with the largest amount of small particles results in the sharpest decrease in the velocity of the gaseous phase.

A distribution in the heat capacity of the solid particles resulted in a minor effect on the velocity of the solid particles and practically no effect on the suspension pressure. The effect on the temperature of solid particles was much more pronounced. As expected, the particles with the smaller heat capacity were heated faster and their temperature reached that of the gaseous phase earlier than those having larger heat capacities.

A distribution in the material density of the solid particles resulted in different velocity and temperature profiles for each of the five solid phases, and a slower rise in the suspension pressure.

Acknowledgement

The financial support received from the U. S. Air Force under Grant AFOSR-86-0349 is acknowledged with thanks.

List of References

Ben-Dor, G. & Igra. O., 1982, J. Plasma Phys., 27, 377.

Carrier, G. F., 1958, J. Fluid Mech., 4, 376.

Elperin, I., Ben-Dor, G. & Igra, O., 1986, ASME J. Fluid Eng., 108, 354.

Gottlieb, J.J. & Coskunses, C.E., 1985, UTIAS Rep. 295.

Igra, O. & Ben-Dor, G., 1980, Israel J. Tech., 18. 159.

Igra, O. & Ben-Dor, G., 1984, J. Plasma Phys., 31, 115.

Kriebel, A.R., 1964, J. Basic Eng., Trans. ASME, D85, 655

Marble, F.E., 1970, Ann. Rev. Fluid Mech., 2, 397.

Morgenthaler, J.H., 1962, in Progress in Astronautics and Rocketry Ed. S. S. Penner & F. A. Williams, Vol. 6, Academic Press, New York, N.Y., p. 145.

Rudinger, G., 1964, Phys. Fluids, 7, 658.

Rudinger, G., 1973, Appl. Mech. Rev., 26, 273.

Sontag, R.E. & Van Wylen, G. J., 1971, Introduction to Thermodynamics, John Willey and Sons

Soo, S.L., 1967, Fluid Dynamics of Multiphase Systems, Blaisdell Publishing Co., Waltham, Mass., U.S.A.

Yum, K.S., Weissman, S. & Mason, E.A., 1962, Phys. Fluids, 5, 672.

Figure Captions

Figure 1: Shock wave structure in pure and dusty gases
Figure 2: Flow field for case 1 of table 1
Figure 3: Flow field for case 2 of table 1
Figure 4: Flow field for case 3 of table 1
Figure 5: Flow field for case 4 of table 1
Figure 6: Flow field for case 5 of table 1
Figure 7: Flow field for case 6 of table 1
Figure 8: Gas properties for cases 1 to 6
Figure 9: Flow field for case 7 of table 1
Figure 10: Flow field for case 8 of table 2
Figure 11: Flow field for case 9 of table 3

Table 1: The loading ratios, η, of the various size particles for $\sigma = 1500$ Kgm/m^3 and C = 1000 J/(Kgm K)

	$D_i \times 10^6$ [m]					Case Number
	5	7.5	10	25	50	M_i
i	1	2	3	4	5	1.5
η	0.04	0.04	0.04	0.04	0.04	1
	0.03	0.04	0.06	0.04	0.03	2
	0.06	0.05	0.04	0.03	0.02	3
	0.02	0.03	0.04	0.05	0.06	4
	0.099	0.06	0.03	0.01	0.001	
	0.001	0.01	0.03	0.06	0.099	6
	-	-	0.20	-	-	7

Table 2: The specific heat capacities, C, of the five various solid phases.
For all the solid phases
$M_0 = 1.5$, $D = 50 \times 10^{-6}$m, $\sigma = 1500$ Kgm/m^3, $\eta = 0.04$

C_i[J/(Kgm K)]					Case Number
1	2	3	4	5	
100	500	1000	5000	10000	8

Table 3: The dust material densities, σ_i, of the five various solid phases.
For all the solid phases
$M_0 = 1.5$, $D = 10 \times 10^{-6}$m, $C = 1000$ J/(Kgm K), $\eta = 0.04$

σ_i[Kgm/m^3]					Case Number
1	2	3	4	5	
1000	1200	1500	1750	2000	9

Table 4: The thermal, l_T, and kinematic, l_V, relaxation lengths for the 9 cases in Tables 1, 2 and 3

Initial Condition in Table	Case Number	l_T [m]	l_V [m]
1	1	1.91	3.83
	2	1.91	3.80
	3	1.90	3.75
	4	1.92	3.90
	5	1.89	3.72
	6	1.92	4.05
	7	0.13	0.31
2	8	37.18	10.4
3	9	0.162	0.39

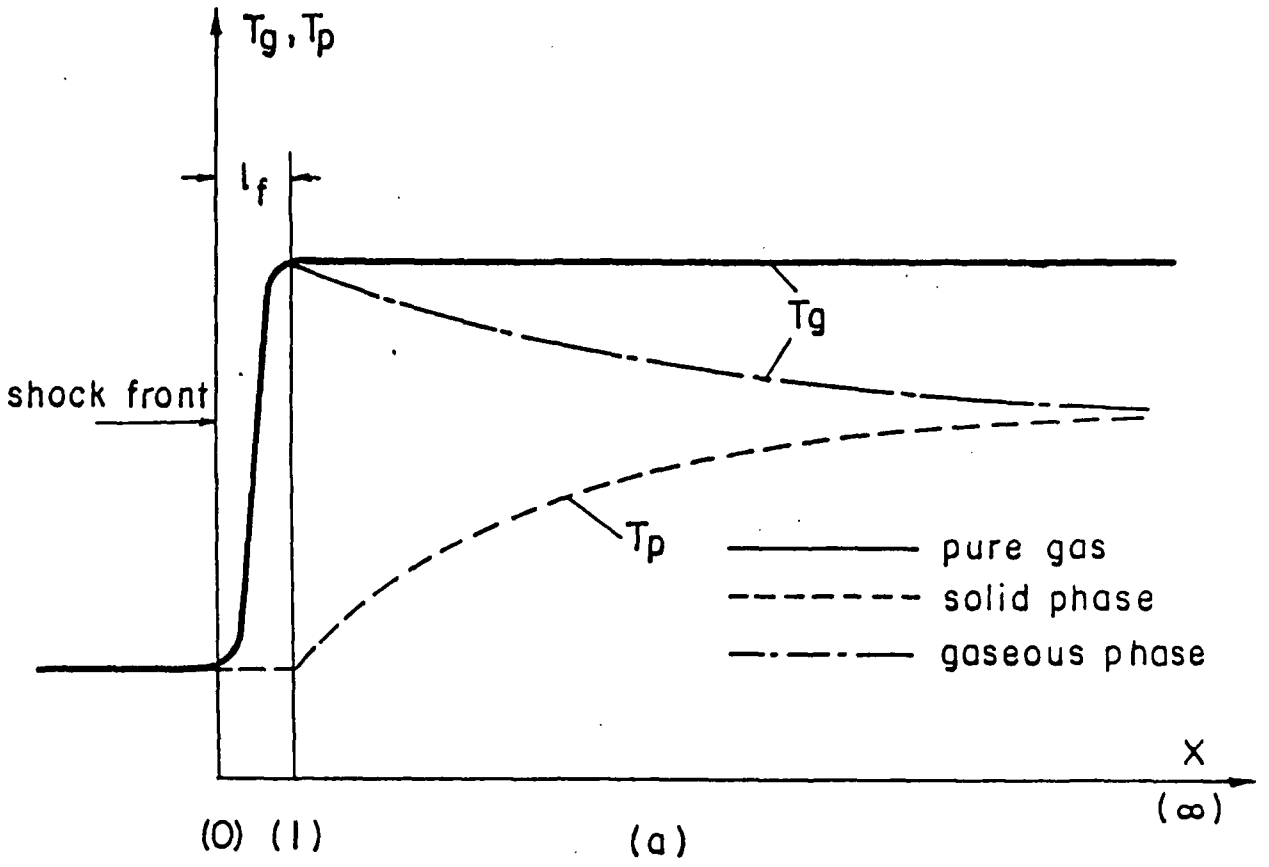
T_g, T_p
l_f
shock front
T_g
T_p
pure gas
solid phase
gaseous phase
X
(∞)
(0) (1)
(a)

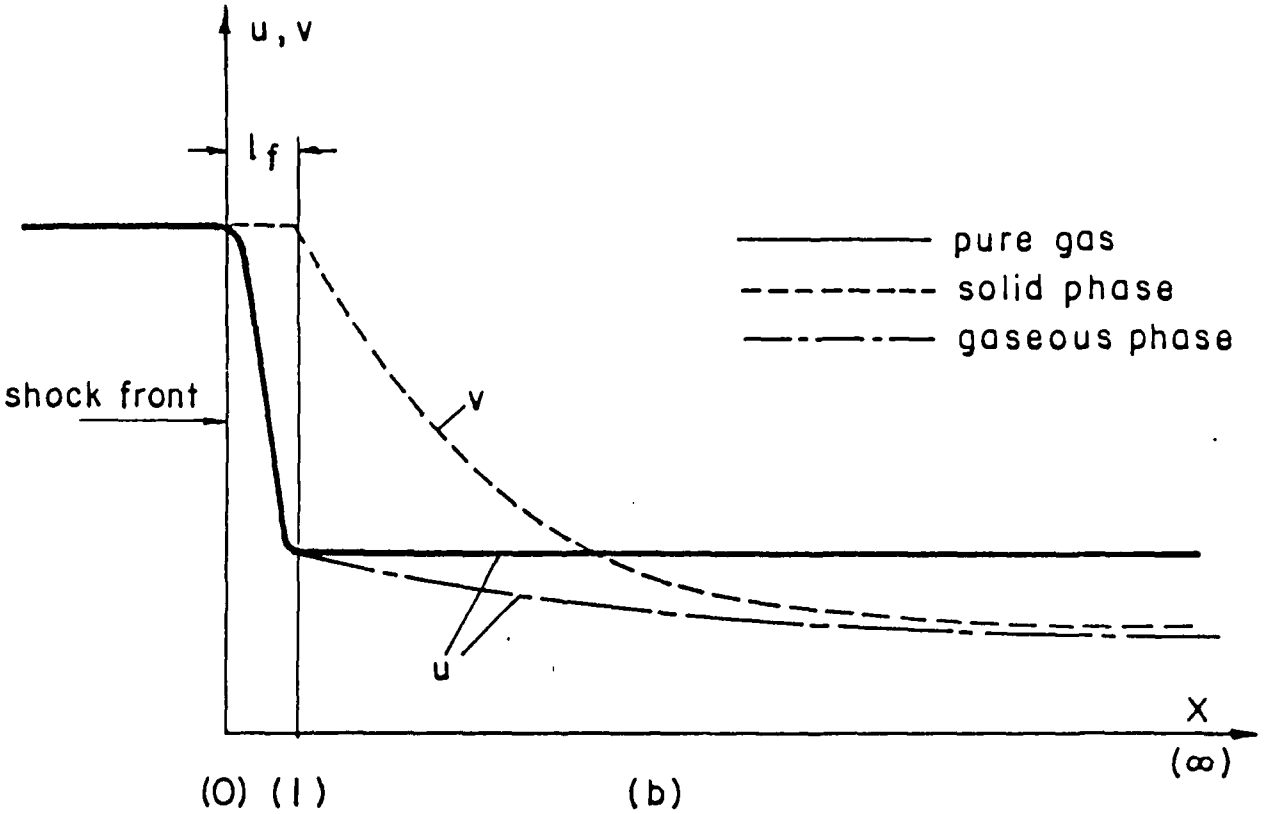
u, v
l_f
shock front
v
u
pure gas
solid phase
gaseous phase
X
(∞)
(0) (1)
(b)

Ελάχιστα ≠ 1

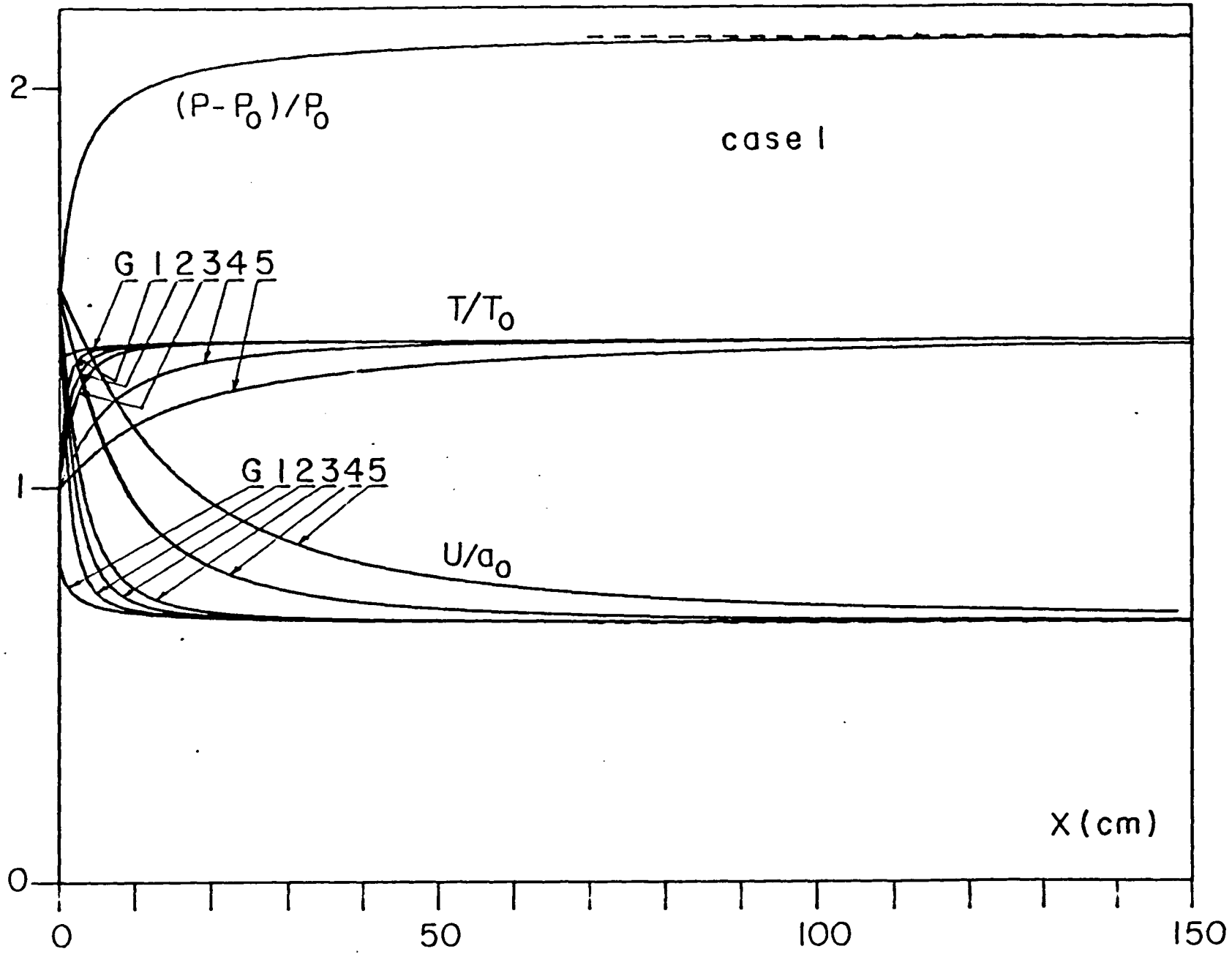
2
1
0
(P-P0)/P0
case 1
G 1 2 3 4 5
T/T0
G 1 2 3 4 5
U/a0
X (cm)
0
50
100
150

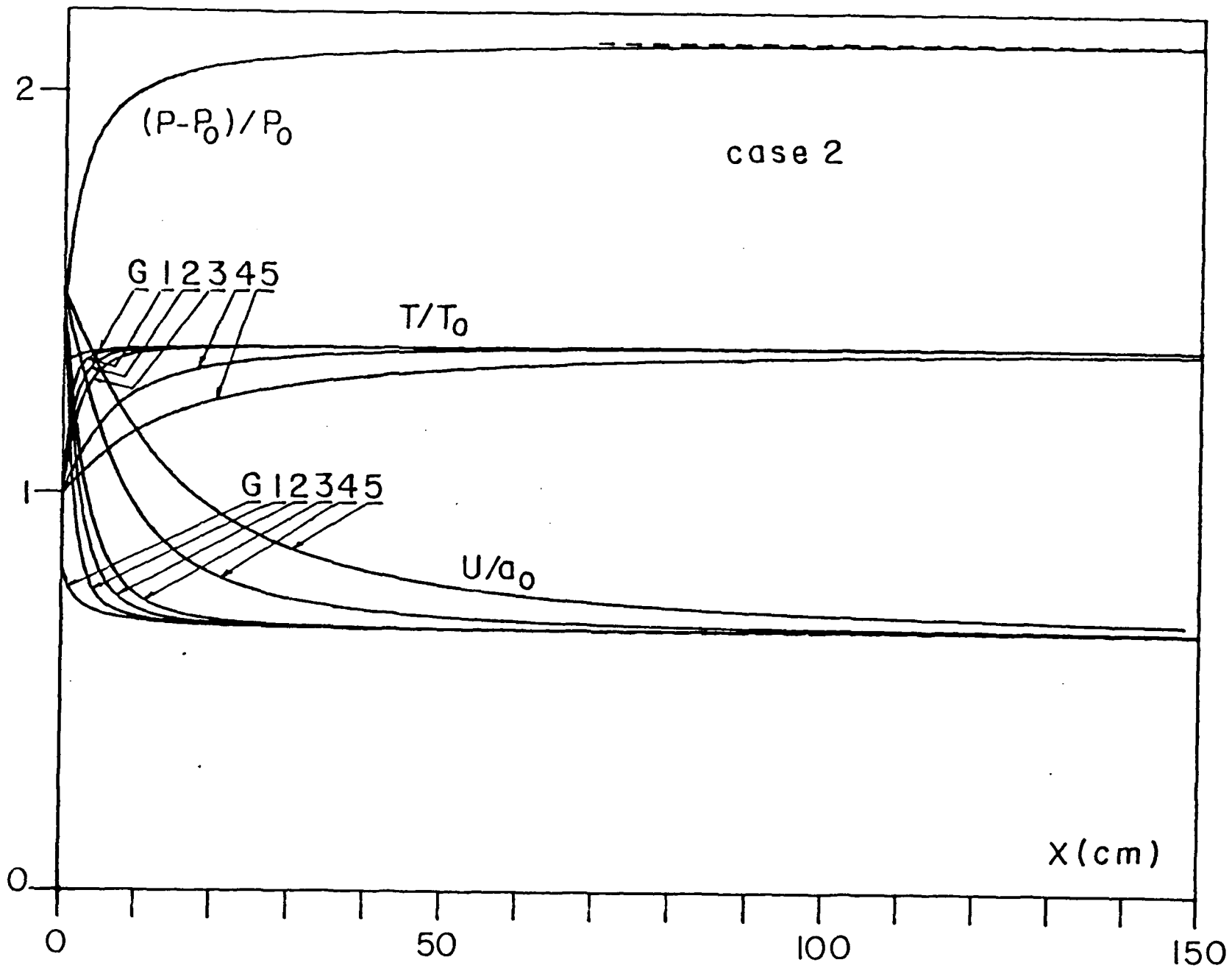
2
1
0
$(P-P_0)/P_0$
case 2
G 1 2 3 4 5
T/T_0
G 1 2 3 4 5
U/a_0
X (cm)
0
50
100
150

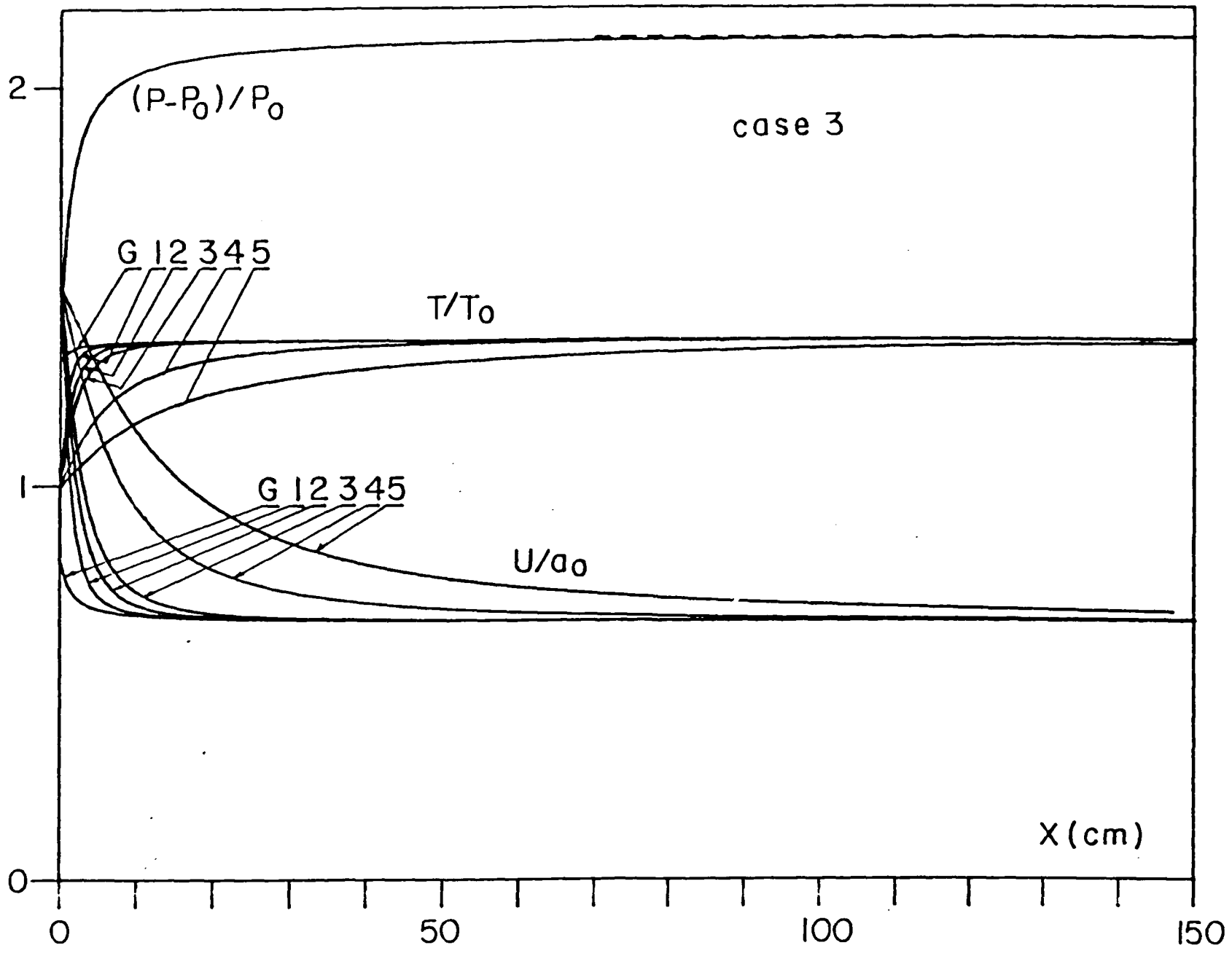
2
1
0
(P-P0)/P0
case 3
G 1 2 3 4 5
T/T0
G 1 2 3 4 5
U/a0
X (cm)
0
50
100
150

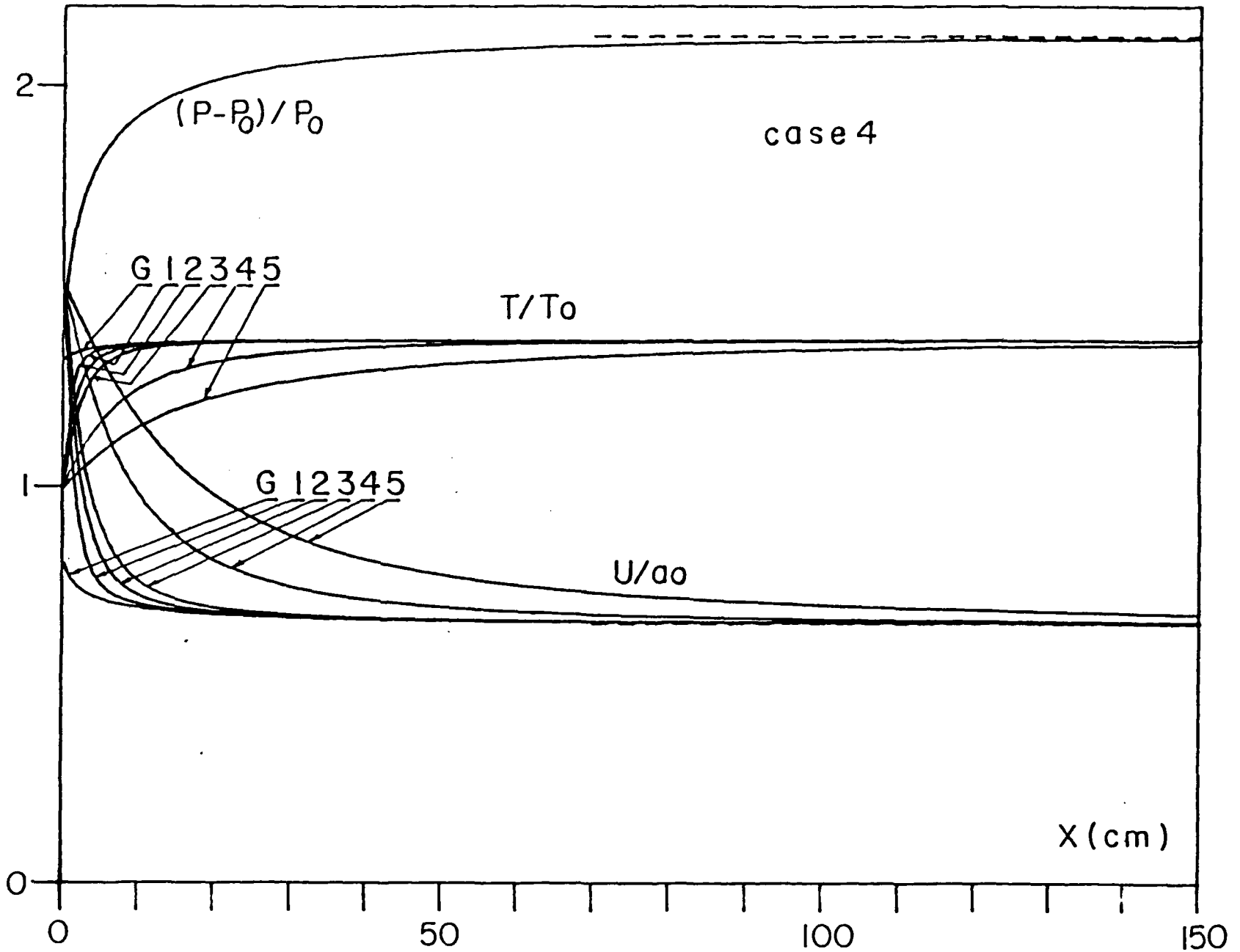
2
1
0
(P-P0)/P0
case 4
G 12345
T/To
G 12345
U/ao
X (cm)
0
50
100
150

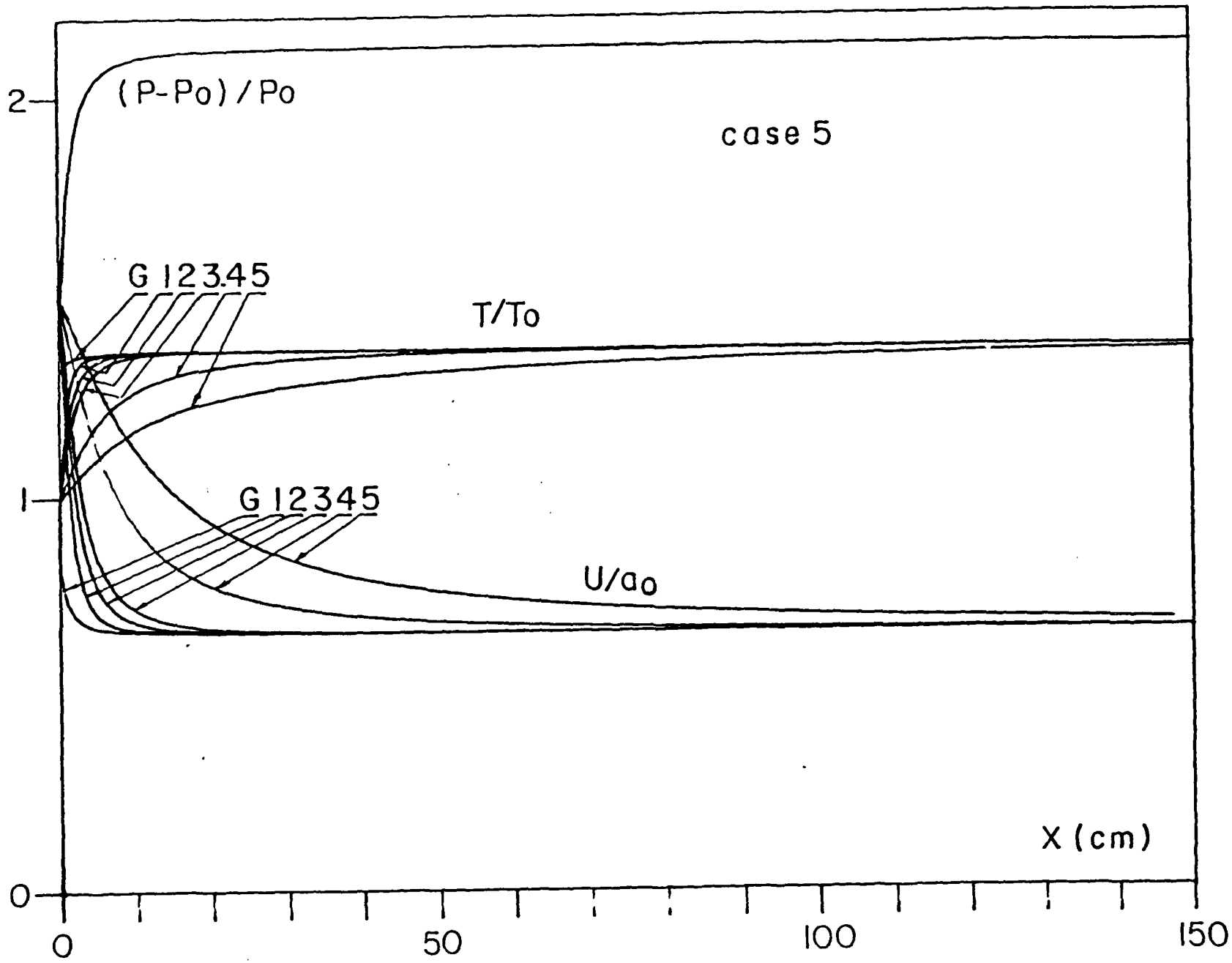
(P-Po) / Po
case 5
G 12345
T/To
G 12345
U/ao
X (cm)
2
1
0
0
50
100
150

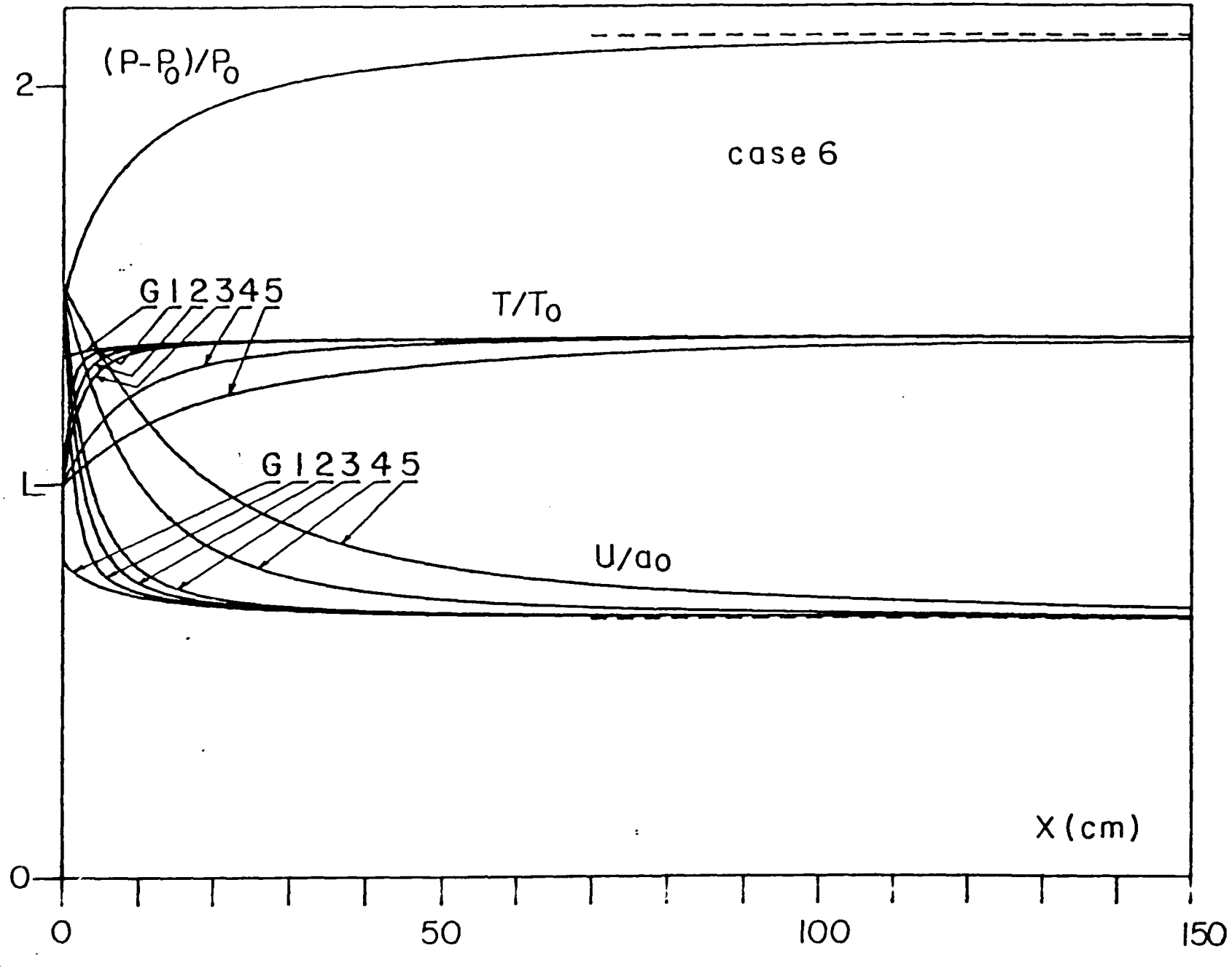
(P-P0)/P0
2
case 6
G12345
T/T0
G12345
L
U/a0
X (cm)
0
0
50
100
150

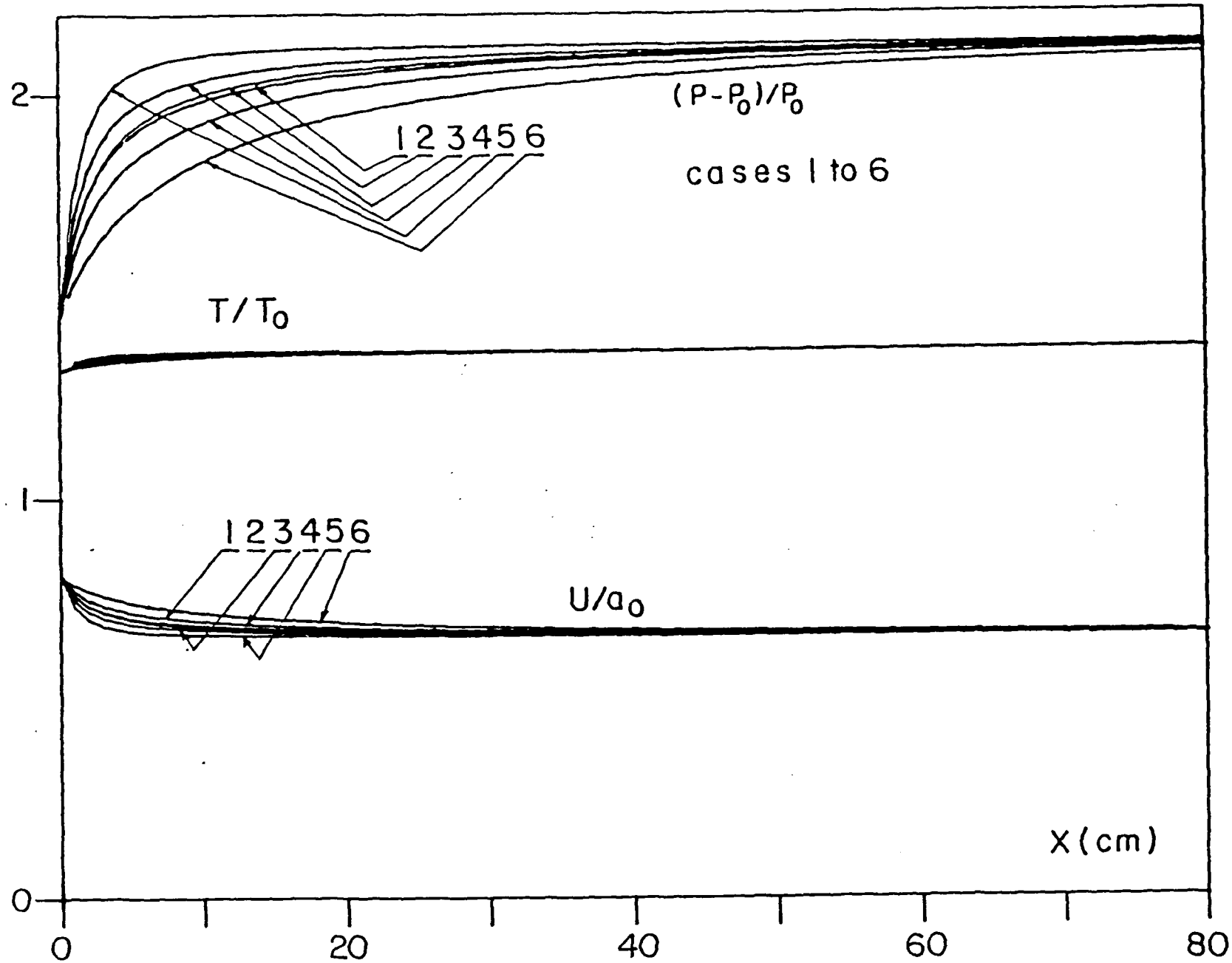
2
1
0
(P-P0)/P0
1 2 3 4 5 6
cases 1 to 6
T/T0
1 2 3 4 5 6
U/a0
X (cm)
0
20
40
60
80

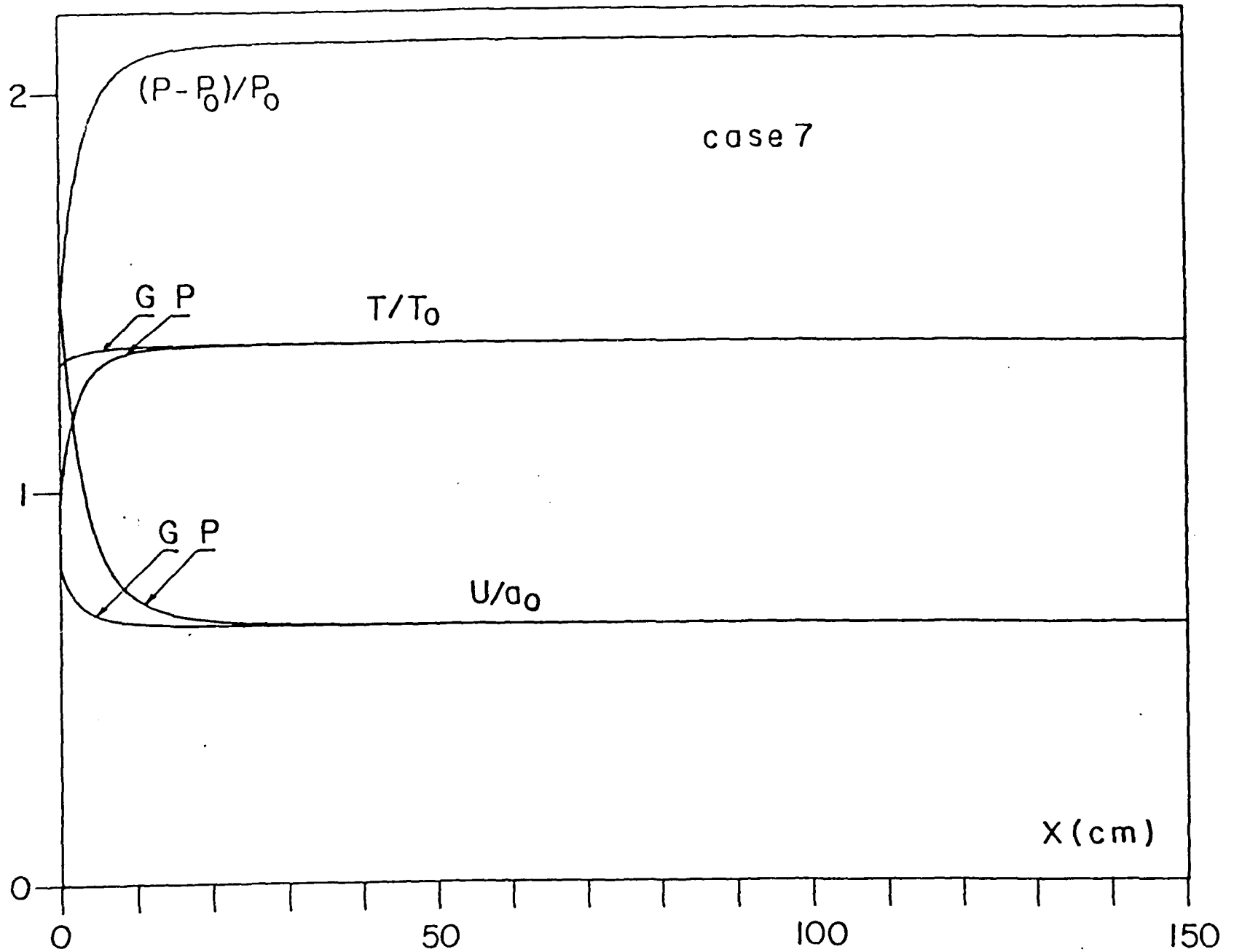
2
1
0
(P-P0)/P0
case 7
G P
T/T0
G P
U/a0
X (cm)
0
50
100
150

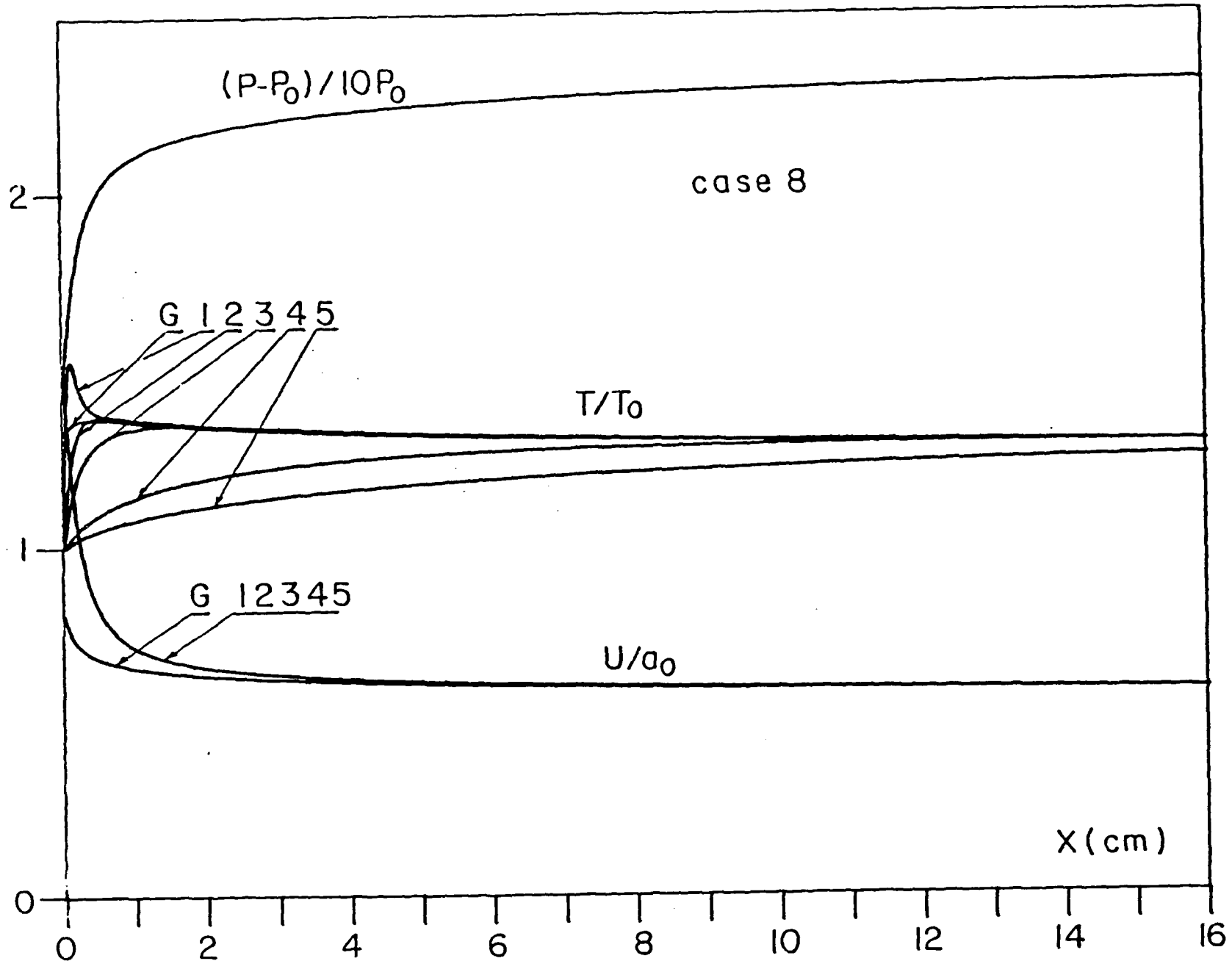
(P-P0)/10P0
case 8
G 1 2 3 4 5
T/T0
G 1 2 3 4 5
U/a0
X (cm)
2
1
0
0
2
4
6
8
10
12
14
16

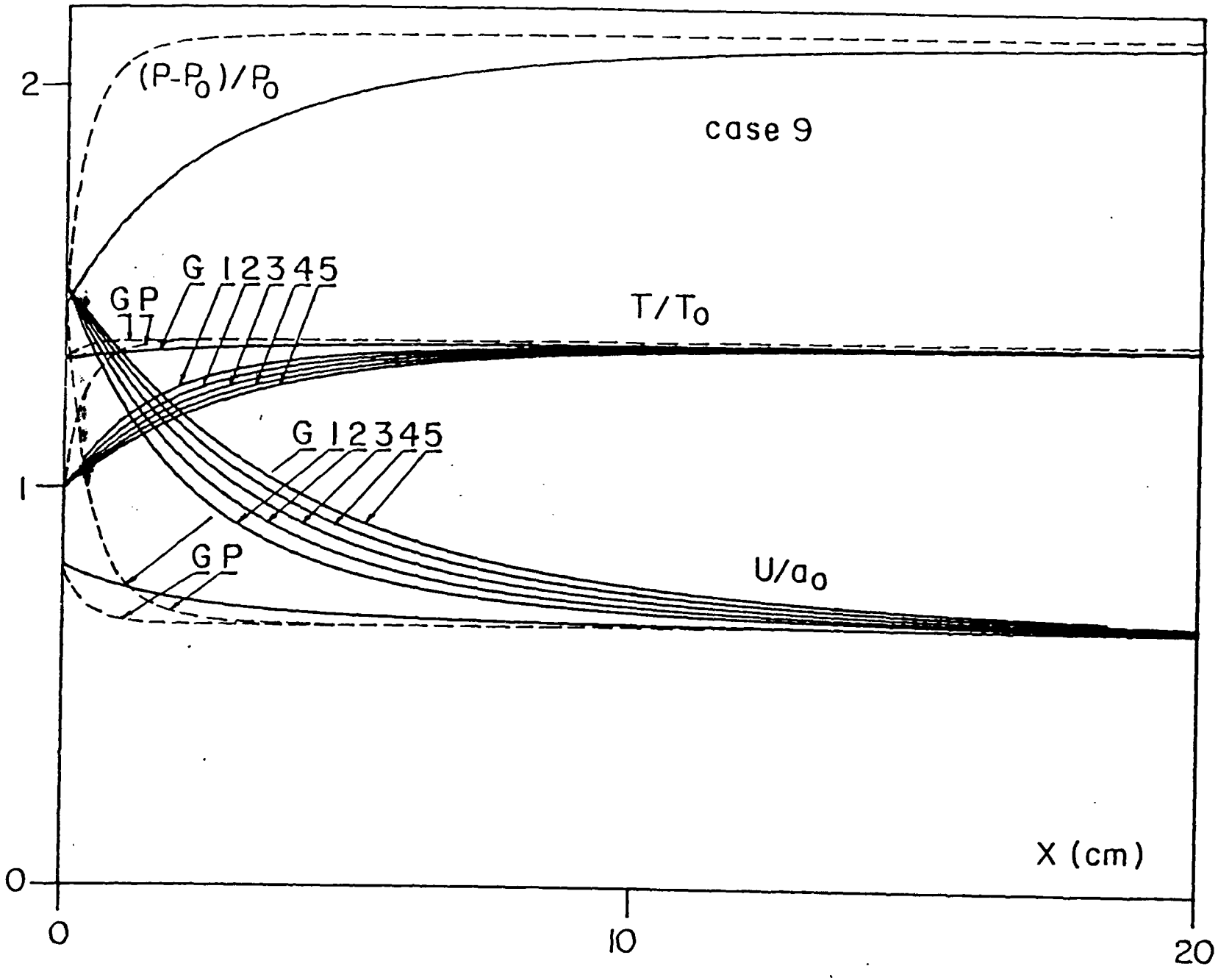
2
1
0
$(P-P_0)/P_0$
case 9
G 12345
GP
11
T/T_0
G 12345
GP
U/a_0
X (cm)
0
10
20